Three Dimensional Numerical investigation of hybrid nanofluids in chain microchannel under electrohydrodynamic actuator

Milad Amiri [1*], Dariusz Mikielewicz [1]

[1] Faculty of Mechanical Engineering and Ship Technology, Gdańsk University of Technology, ul. Gabriela Narutowicza 11/12, 80-233 Gdańsk, Poland

Corresponding Authors:

milad.amiri@pg.edu.pl

Three Dimensional Numerical investigation of hybrid nanofluids in chain microchannel under electrohydrodynamic actuator

Abstract

Energy efficiency enhancement methods have received considerable attention within the industry and scientific community, owing to the rising concern of global energy sustainability. The present paper attempts to scrutinize the effects of electrohydrodynamics and nanofluids on the rate of heat transfer and fluid flow in the 3D chain microchannels. Improved heat exchangers (e.g., chain microchannel) would have a key role in increasing of the performance of such systems since they provide efficient thermal management needed for more robust computational power. To date, analysis of electrohydrodynamics and nanofluids in the chain microchannel was not comprehensively discussed. Here, steady-state, laminar and three-dimensional chain microchannel are numerically modeled based on a control volume method in Fluent. Results show that by increasing the volume fraction of nanoparticles, the viscosity of the nanofluid increases leading to an increase in pressure drops. Moreover, Nusselt at Re = 125, 250, 500 and 1000 for hybrid nanofluid ($\emptyset_{AL2O3} = \emptyset_{CuO} = 4\ \%$) is 1.206, 1.541, 2.075 and 2.707, respectively which, in turn, depicts surging by 22.94%, 24.17%, 24.70% and 24.707% in comparison to water, respectively. In addition, at low Reynolds number ($0.416 \leq Re \leq 4.166$), the lower Reynolds results in decreasing of percentage of pressure drop. Meanwhile, imposing electrohydrodynamic (V=30 KV) at Re= 125, 250, 500 and 1000 leads to increasing by 23%, 22%, 20% and 18% of Nusselt number in comparison to absence of electric field, respectively. It means that the considered effect of the increasing the Nusselt number at lower Reynolds number is more effective. Moreover, heat transfer rises with augmentation of supplied voltage and Reynolds number.

Keywords

Numerical modeling, Chain microchannel, EHD, Hybrid nanofluid, Fluid flow, Three dimensional

1. Introduction

Multiple techniques can be used to achieve higher heat transfer rates in microchannels, which leads to considerable energy savings owing to smaller designed systems and more efficient equipment for assembling governing loads [1]. Systems with higher efficiency need to be developed to manage the heat excess issue and decrease material consumption. In this regard heat exchangers are among the main systems commonplace in numerous industries. Heat exchangers are being used in nuclear power generation and thermoelectric[2-7], pharmaceutical drug development [8], food preparation [9], refrigeration [10], building energy technology [11] agriculture [12], transportation [13], material processing [14, 15], petrochemical processing [16], bulk materials manufacturing [17, 18], and many more. Moreover, it is possible to manufacture a heat exchanger of a smaller size with the same performance (as an equivalent heat transfer) to cut material costs and increase volumetric power density at the same time. Improved heat exchangers would have a key role in heightening the performance of such systems since they provide efficient thermal management needed for more robust computational power. The heat transfer efficiency can be enhanced in heat exchangers using several methods., e.g., using extended surfaces, applying vibration to the heat transfer surfaces, and using microchannels [19]. Particularly, microchannels are reliable solutions in many micro-scale applications since they are capable of absorbing or dissipating vast heat quantities[20-22].

Heat transfer can be enhanced for internal single-phase flows using three techniques, namely active, passive, and a combination of active and passive. Passive methods can operate without needing external input such as mechanical actuation or electrical power[23]. Given the available heat exchanger technologies, such methods are highly common for heat transfer enhancement because of their low integration penalty. Passive techniques have been founded on raising thermal conductivity (with the use of nanoparticles) or changing the geometry of the heat transfer component (e.g., tube) through inserts addition or changing the walls of the tubing. Among these techniques, one can highlight dimples, tape inserts, and wire inserts. On the contrary, external input is required for active methods to be able to operate. Generally, active methods have more complexity and costs and have not been used as broadly as passive methods. However, heat transfer enhancement can be controlled by active methods. Our paper aims to use a combination of active and passive techniques, i.e., nanoparticles addition as the passive technique and using electrohydrodynamic (EHD) as the active enhancement.

As a great active method for heat transfer improvement, EHD employs an electric field for disturbing the boundary layer of a dielectric fluid. In other words, radial fluid motion is induced by electric fields, which causes the anticipated disturbance in the boundary layer. In this regard, Kasayapanand et al. [24]studied the effect of various electrode arrangements on heat transfer, concluding that ionic wind elevated the temperature gradient. Sheikholeslami et al. [25]reported the impact of electric field on nanofluid convective heat transfer. Also, Sheikholeslami and Chamkha [26]investigated the electric field impact on Fe_3O_4 – H_2O free convection behavior,

concluding flow style can be changed by Coulomb forces. The electro viscous effect was investigated by Jing and Pan [27] investigated on convective heat transfer in a tube, showing that a higher decrease in Nusselt number can be observed due to the slip effect on surface charge. Electric field can also use inside the geometry of drying [28-30]. The electric field impact on nanofluid forced convection was studied by Sheikholeslami and Ellahi [31]. Results depicted that the flow shape was changed by supplied voltage. Many studies have been carried out [32-35] or numerically [36-39] , mainly on the turbulent flow approach. Experimental studies concerning flow velocity measurements chiefly benefit from three main techniques, including Particle Image Velocimetry (PIV), Hot Wire Anemometry, and Laser Doppler Anemometry (LDA), which have shown some uncertainties because of the electric field impact on the measurement process. Accordingly, numerical simulation of the EHD cases should be crucially addressed and, in turn, it is substantially required to adopt robust approaches for the induced flow dynamic behavior. A direct numerical simulation (DNS) was conducted by Soldati and Banerjee [36] for the flow field in a wire-channel based on superimposition of the turbulence induced by electric field excitations and hydrodynamic turbulence of the main flow. They illustrated that even hydrodynamically laminar flow tended towards turbulent instabilities close to the excited areas when affected by corona winds [40] Working fluid's thermal conductivity can be increased to improve heat transfer. Compared to the thermal conductivity of solids, heat transfer fluids that have been commonly used (such as water, engine oil, and ethylene glycol) have relatively low thermal [41]. Thus, small solid particles can be added to the fluid to increase its thermal conductivity. Several researchers have studied the possibility of using such suspensions of solid particles (with sizes on the order of 2 mm or micrometers), where serious drawbacks were observed [42]. Nanofluid is defined as a uniform and stable suspension with solid nanoparticles, typically with a size of 1–100 nm in size [43]. Nanofluid has been highly addressed over the past decade in the heat transfer community. Given its capability to improve the thermal proprieties of the original fluid, several studies have applied single-phase heat transfer enhancement in recent years [44-46]. As per the material of nanoparticles, nanofluids can be categorized into metal oxides (e.g., Al_2O_3, ZnO, SiO_2, TiO_2, Fe_2O_3), stable metals (e.g., silver, gold, and copper), and different forms of carbon and carbon oxides (e.g., graphite. diamond, and nanotubes). Various kinds of nanoparticles have been employed for different applications. Boussoufi and Sabeur studied flow characteristics of natural convective nanofluid with Brownian motion effect inside an annular space within confocal elliptic cylinders [47]. Sheikholeslami and Ganji [26, 48] used nanofluid as a passive approach and proposed innovative numerical and analytical methods. Results found that the Nusselt number is a diminishing function of Hartmann number. Bouhalleb and Abbassi [49] investigated the effect of the tilted angle on the velocity and temperature profiles, revealing that the temperature gradient was augmented by increasing nanofluid volume fraction. Rotating nanofluid flow that was induced by an exponentially stretching plate was investigated by Ahmad and Mustafa [50], revealing that the temperature gradient was reduced by increasing angular velocity. Bouhalleb and Abbassi [51] examined the heat transfer of CuO-water nanofluid in a titled cavity, showing changing aspect ratio was more influential at higher buoyancy forces.

Hybrid nanofluids contain different types of nanoparticle materials (more than one), which have been considered to enhance heat transfer a subcategory of coupled methods. Much attention has been directed toward hybrid nanofluids due to their capability to improve thermal characteristics, outperforming normal nanofluids [44, 52, 53]. Nonetheless, obtained results have revealed that it is very challenging to select suitable hybrid nanoparticles to prepare stable nanofluids [54, 55]. Also, the majority of the current studies on hybrid nanofluids have focused on single-phase heat transfer enhancement.

In this paper, heat transfer enhancement effects that combine presence of nanofluid and EHD methods is considered. Several researchers utilized a combined method for heat transfer improvement [56-61] To obtain a numerical model and optimize the nanofluid-based chain microchannel, firstly, different types of nanofluid including Al_2O_3-water, CuO-water and hybrid nanofluid should be defined. Then, a suitable type of nanofluid can be obtained using distribution of pressure and Nusselt number. Next, the numerical simulation on different value of volume fraction of hybrid nanofluid is conducted, and by applying 0% up to 4% of volume fraction for hybrid nanofluid, the model is derived. After obtaining the model, the behaviour of the nanofluid-based chain microchannel affected by EHD can be estimated, and the effect of hybrid nanofluid at low Reynold numbers of the chain microchannel can be presented. Finally, using both EHD and hybrid nanofluid optimization, the optimum value of the voltage of EHD can be calculated.

2. Modeling

Figure 1 shows the geometry of a three-dimensional passive microchannel. Although this type of microchannel can be used as a micromixer on the basis of split and recombination (SAR), in this paper it is used as a microchannel. The main operating principle of this sort of microchannel is to rotate a flow 90 degrees and fold the stream to increase the microchannel's efficiency. During the microchannel, this process is continued until the appropriate degree of parameters is achieved. After each vertical section, the new part has a diameter of 0.6 mm and is expanded by 0.2 mm rather than the outflow of the vertical section (0.4mm), as shown in Fig.1. The diameter of the segment outlet is 0.4 mm, like the vertical section. The maximum and minimum width of the microchannel is 0.6 mm and 0.4 mm, respectively. As seen in the chain microchannel in Fig.1, flows enter at the entrance of the microchannel and move along the entrance section until they meet the vertical section. At the end of the vertical part the stream attains the first chain element.

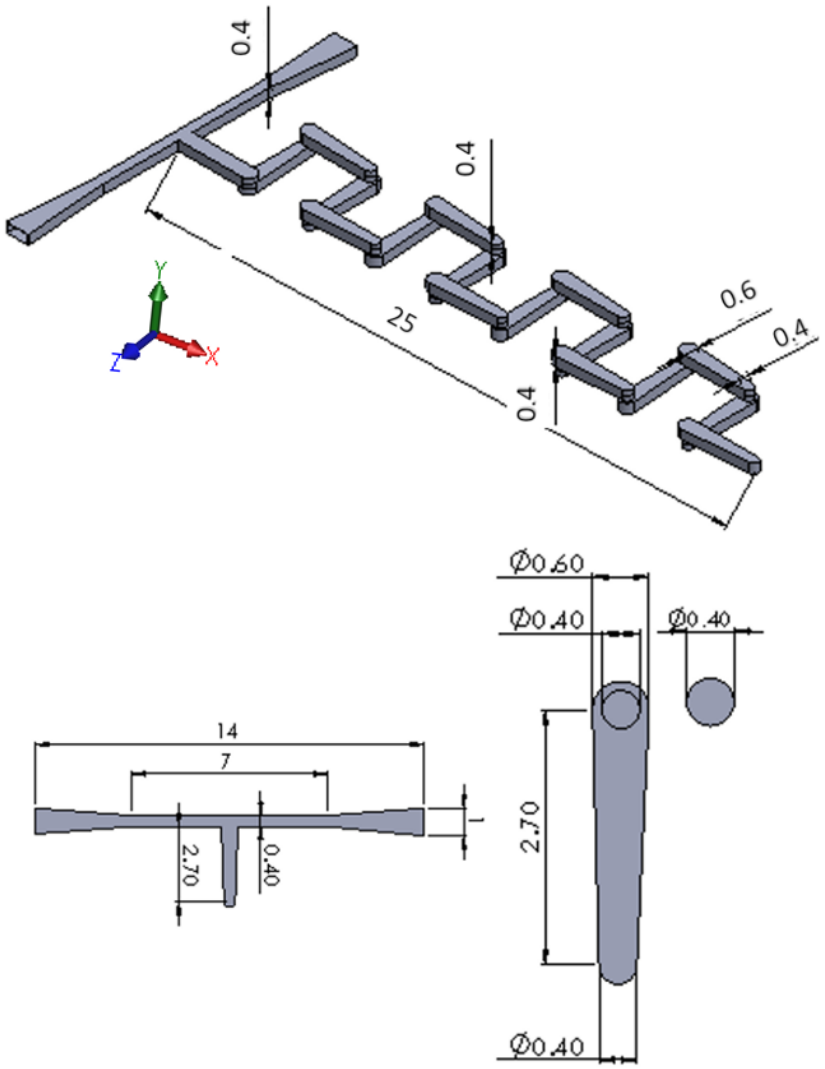

2.1 Modeling for thermo-physical properties of nanofluids

Nanofluids' thermo-physical properties are crucial for predicting the behavior of their heat transfer. It is extremely momentous in terms of the energy saving and industrial perspectives. Nanoparticles have superb potential to enhance the thermal transport properties in comparison to conventional particles such as fluids suspension, micrometer and millimeter sized particles. In the recent decades, nanofluids have received significant attention because of their enhanced thermal properties [19]. Experimental investigations illustrate that nanofluids' thermal conductivity depends on many parameters such as particle material, particle volume fraction, particle shape, particle size, temperature and base fluid material. Types and amount of acidity and additives of the nanofluid were also depicted to be affective in enhancement of the thermal conductivity [19]. The equations applied for the density, specific heat, viscosity and thermal conductivity estimation have been summarized as follows.

Density is described as follows [62, 63]:

$$\rho_{nf} = (1 - \emptyset_s)\rho_{bf} + \emptyset_s\rho_s \quad (1)$$

where $\emptyset_s$ and ρ refer to the volume fraction of particles and density, respectively. The subscripts denote base-fluid, nanofluid, and nanoparticle i.e. bf, nf and s, respectively.

Specific heat of nanofluid is determined from [64, 65]:

$$(\rho C_p)_{nf} = (1 - \emptyset_s)(\rho C_p)_{bf} + \emptyset_s(\rho C_p)_s \quad (2)$$

Dynamic viscosity is described by [66]:

$$\mu_{nf} = \frac{\mu_{bf}}{(1 - \emptyset_s)^{2.5}} \quad (3)$$

Thermal conductivity can be specified as [67]:

$$\frac{k_{nf}}{k_{bf}} = \frac{k_s + 2k_{bf} - 2\emptyset_s(k_{bf} - k_s)}{k_s + 2k_{bf} + \emptyset_s(k_{bf} - k_s)} \quad (4)$$

Maxwell's formula depicts that the nanofluids' effective thermal conductivity depends on the base fluid, the thermal conductivity of the particle and the volume fraction of the solid particles.

2.2 Modeling of thermo-physical properties of hybrid nanofluid

The thermo-physical characteristics of nanofluids have been determined using classical models. These models, however, do not provide the accurate values of thermophysical properties for the hybrid nanofluid. Nevertheless, different experimental results allow us to adopt more precise model for describing thermos-physical properties of hybrid nanofluid. The density of hybrid nanofluid is expressed by Eq. (5):

$$\rho_{hnf} = \emptyset_{Al_2O_3}\rho_{Al_2O_3} + \emptyset_{CuO}\rho_{CuO} + (1 - \emptyset)\rho_{bf} \quad (5)$$

where $\emptyset$ is the overall volume concentration of two different types of nanoparticles dispersed in a base fluid in the hybrid nanofluid and is achieved as follows:

$$\emptyset = \emptyset_{Al_2O_3} + \emptyset_{CUO} \quad (6)$$

According to Eq. (2), the heat capacity of hybrid nanofluid is obtained by following calculation:

$$C_{hnf} = \frac{\emptyset_{Al_2O_3}\rho_{Al_2O_3}C_{Al_2O_3} + \emptyset_{CuO}\rho_{CuO}C_{CuO} + (1-\emptyset)\rho_{bf}C_{bf}}{\rho_{hnf}} \quad (7)$$

Equation (8) was suggested by Hamilton and Crosser [68], where n is the empirical shape factor that accounts for the impact of shape of particles and can range from 0.5 to 6.0. The shape factor n is equal to $\frac{3}{\varphi}$, where φ is the particle sphericity, which is defined as the ratio of sphere's surface area to the particle's surface area. For spherical nanoparticle n is equal to 3. The Hamilton and Crosser model (n = 3) is identical to the Maxwell model (Eq. (4))

$$\frac{k_{nf}}{k_{bf}} = \frac{k_s + (n-1)k_{bf} - (n-1)\emptyset_s(k_{bf} - k_s)}{k_s + (n-1)k_{bf} + \emptyset_s(k_{bf} - k_s)} \quad (8)$$

The thermal conductivity of Al_2O_3–CUO/water (hybrid nanofluid) is defined using the Maxwell model (Eq. (4)), which is a general equation for determining the thermal conductivity of a mixture including a base fluid and dispersed solid particles. As a result, Eq. (9) derived from Maxwell equation, will be used for k_{hnf}.

$$\frac{k_{hnf}}{k_{bf}} = \frac{\frac{(\emptyset_{Al_2O_3}k_{Al_2O_3} + \emptyset_{CUO}k_{CUO})}{\emptyset} + 2k_{bf} + 2(\emptyset_{Al_2O_3}k_{Al_2O_3} + \emptyset_{CUO}k_{CUO}) - 2\emptyset k_{bf}}{\frac{(\emptyset_{Al_2O_3}k_{Al_2O_3} + \emptyset_{CUO}k_{CUO})}{\emptyset} + 2k_{bf} - (\emptyset_{Al_2O_3}k_{Al_2O_3} + \emptyset_{CUO}k_{CUO}) + \emptyset k_{bf}} \quad (9)$$

2.3 Governing equations

The following are the governing equations for the electric field and micropolar fluid. The simplified assumptions for the governing equations are as follows:

1. The field of electrical and velocity is laminar and steady.
2. Flow is incompressible and Three-dimensional.
3. Fluid is Newtonian and isentropic.
4. Viscous dissipation is negligible.
5. The magnetic field is neglected.
6. Buoyancy force and free convection are neglected.
7. The nanoparticles are uniformly dissolved throughout the mixture and considered as a single phase.Therefore, the speed of slip is zero and its effects are not considered.

2.3.1 Modeling for electric field

The EHD enhancement method results from the electric force density (body force) acting on the molecules of a dielectric fluid in the presence of an electric field, which comprised of three terms.

$$\overrightarrow{F_e} = \rho_c \vec{E} - \frac{1}{2}\vec{E}^2 \nabla \varepsilon_s + \frac{1}{2}\nabla\left[\vec{E}^2 \rho\left(\frac{\partial \varepsilon_s}{\partial \rho}\right)\right] \quad (10)$$

Where $\vec{E}$ and ρ_c refer to electric field strength vector (V/s) and charge density (C/m^3), respectively. ε_s is dielectric permittivity (F/m). The first term represents the impact of the electric field on free charges, namely the electrophoresis or Coulomb force. The second and the third terms depict dielectrophoresis and electrostriction force densities, which are referred to as polarization forces induced in the field [69]. Due to the constant electric permittivity, the second and third terms on the right side of Eq. (10) become neglectable. As a result, the electrohydrodynamic force is limited to Coulomb force ($\rho_c \vec{E}$) which is used as a source term in the momentum equation. The electrohydrodynamic governing equations were calculated as follows [40].

Poisson's equation expressed as:

$$\nabla^2 V = -\frac{\rho_c}{\varepsilon_s} \quad (11)$$

V refers to electric potential (V).

The electric field has been formulated as:

$$\vec{E} = -\nabla V \quad (12)$$

The current continuity equation is:

$$\nabla . \vec{j} = 0 \quad (13)$$

Where j is the electric current density (A/m^2) as its shown:

$$\vec{j} = \rho(\rho_c \beta \vec{E} + \rho_c \vec{u} + D_e \nabla \rho_c) \quad (14)$$

β and $\vec{u}$ are ion mobility (m^2/(V·s)) and velocity vector (m/s), respectively. D_e specifies diffusion coefficient of ions (m^2 /s). Three variables on the right side of Eq. (14) depict drift, convection and diffusion of electric charges, respectively. It should be noted that the diffusion of electric charges ($D_e \nabla \rho_c$) is very negligible in micro-scale ionic flows and can be ignored. For air, the charge

convection term in Eq. (14) ($\rho_c\vec{u}$) is about two orders of magnitude smaller than ions' drifting term ($\rho_c\beta\vec{E}$), whilst it is not appropriate assumption for liquids. Because ion mobility is very low in liquids, whereas in air and other gases it is high and $\frac{u}{\beta E}$ is order of 0.1 or less than 0.1. So, mentioned term ($\rho_c\vec{u}$) is considered owing to used fluids (water and nanofluids) in this paper.

According to these assumptions, the electric current density has been reformulated as follows:

$$\nabla.(\rho_c\mathbf{u} - \rho_c\beta\nabla V) = 0 \tag{15}$$

Therefore, Eqs, (11) and (15) are the main equations governing electrohydrodynamic effect. In order to analyse the electrical body force, these equations must be simultaneously solved.

2.3.2 Modeling of micropolar fluid

The governing equations of the micropolar fluid model by assuming three-dimensional, a steady state, incompressible flow and laminar affected by EHD-induced force, is affirmed as:

Continuity:

$$\mathrm{div}(\vec{u}) = 0 \tag{16}$$

Momentum:

It is assumed that viscosity buoyancy force and dissipation are neglected.

$$\nabla\left(\rho_{nf/hnf}\vec{u}.\vec{u}\right) = \nabla.\mu_{nf/hnf}\nabla\vec{u} - \nabla P + \rho_{nf/hnf}\vec{g} + \rho_c E \tag{17}$$

$nf or\ hnf$ refers to thermo-physical properties of nanofluid or hybrid nanofluid.

Energy:

$$\nabla\left(\rho c_{p_{nf/hnf}}\vec{u}T\right) = \nabla.\left(k_{nf/hnf}\nabla T\right) + \vec{J}.\vec{E} \tag{18}$$

2.4 Modeling of UDF, UDS and UDM

As the state of the art of CFD methodology, the commercial software FLUENT is a powerful computational package which is widely used in the industrial and academic field to simulate heat transfer and fluid flow. However, it does not have a default module to assist users in analyzing

electrohydrodynamic phenomena. In this paper, simulation of chain microchannel in FLUENT based on its UDF (User Defined Function), UDM (User define Memory) and UDS (User Defined Scalar) has been developed.

The electric current density and Poisson's equations (Eqs, (11) and (15)) are defined by the user defined scalar (UDS) to obtain ρ_c and V.

Solving the transport equations for an arbitrary is useful for both single phase and multiphase flow. Used fluids in this paper have been considered single phase flow by using thermo-physical properties of nanofluids and hybrid nanofluid. So, UDS for single phase flow will be elaborated in line with the procedure outlined below.

For an arbitrary scalar ζ_k, ANSYS FLUENT solves the equation

$$\frac{\partial \rho \zeta_k}{\partial t} + \frac{\partial}{\partial x_i}\left(\rho u_i \zeta_k - \Gamma_k \frac{\partial \zeta_k}{\partial x_i}\right) = S_{\zeta_k} \quad k=1,..., N \tag{19}$$

Where S_{ζ_k} and Γ_k refer to the source term and diffusion coefficient supplied for each of the N scalar equations. Γ_k is described as a tensor in order to an isotropic diffusivity. The diffusion term is thus $\nabla.(\Gamma_k.\zeta_k).\Gamma_k$, for isotropic diffusivity, could be inscribed as $\Gamma_k I$ where I refer to the identity matrix. Depending on the approach used to determine the convective flux, one of the three following equations will be solved by ANSYS FLUENT for the steady-state state:

1. Without computing convective flux, following equation will be solved by Fluent:

$$-\frac{\partial}{\partial x_i}\left(\Gamma_k \frac{\partial \zeta_k}{\partial x_i}\right) = S_{\zeta_k} \quad k=1,..., N \tag{20}$$

2. With computing convective flux with mass flow rate, following equation will be solved by Fluent:

$$\frac{\partial}{\partial x_i}\left(\rho u_i \zeta_k - \Gamma_k \frac{\partial \zeta_k}{\partial x_i}\right) = S_{\zeta_k} \quad k=1,..., N \tag{21}$$

To add Eqs. (11) and (15) in Fluent, cases 1 and 2 have been used, respectively. Then, UDM is written to achieve E from Eq. (12). Then, UDF is used to solve source term.

2.5 Boundary conditions

The boundary conditions are divided into two parts including flow field and electric field. The flow and electric boundary conditions are explained in table1.

Table1. flow and electric boundary conditions

Border	Flow	Temperature	Electric potential	Electric charge
Flow inlet	Velocity inlet ($\boldsymbol{u} = u_\infty$)	80 (℃)	$\frac{\partial V}{\partial n} = 0$	$\frac{\partial \rho_c}{\partial n} = 0$
Flow outlet	Pressure outlet	27 (℃)	$\frac{\partial V}{\partial n} = 0$	$\frac{\partial \rho_c}{\partial n} = 0$
Electrode	$\boldsymbol{u} = 0$ (No Slip)	$\frac{\partial T}{\partial n} = 0$	$V=V_0$	$\rho_c=\rho_{c_0}$
Surface electrode	$\boldsymbol{u} = 0$ (No Slip)	27 (℃)	V=0	$\frac{\partial \rho_c}{\partial n} = 0$
Other surfaces	$\boldsymbol{u} = 0$ (No Slip)	27 (℃)	$\frac{\partial V}{\partial n} = 0$	$\frac{\partial \rho_c}{\partial n} = 0$

3. Evaluation of numerical model

ANSYS Fluent 2021 R1 was utilized to estimate properties like flow pattern for the examined microchannel. Fluids enter through two inputs, mix inside the channel and then exit from the microchannel's output. In the present calculation, the different properties were specified for the fluids. The value of Reynolds numbers was determined as one of the preliminary parameters for this investigation and is specified as:

$$Re = \frac{\rho u d}{\mu} \tag{22}$$

Where u is the fluid velocity, ρ and μ are the fluid density and dynamic viscosity, respectively, and d is the characteristic length.

3.1 Grid Independence

Figure 2 depicts the geometry of chain microchannel and its mesh. For meshing the created model, all the edges were meshed in order to increase the accuracy of calculations. After that, all the faces and volumes were meshed. In the case of meshing, Tet/Hybrid elements and TGrid type was used

to generate cells suitable for the complex geometry used in computational fluid dynamics (CFD) simulations.

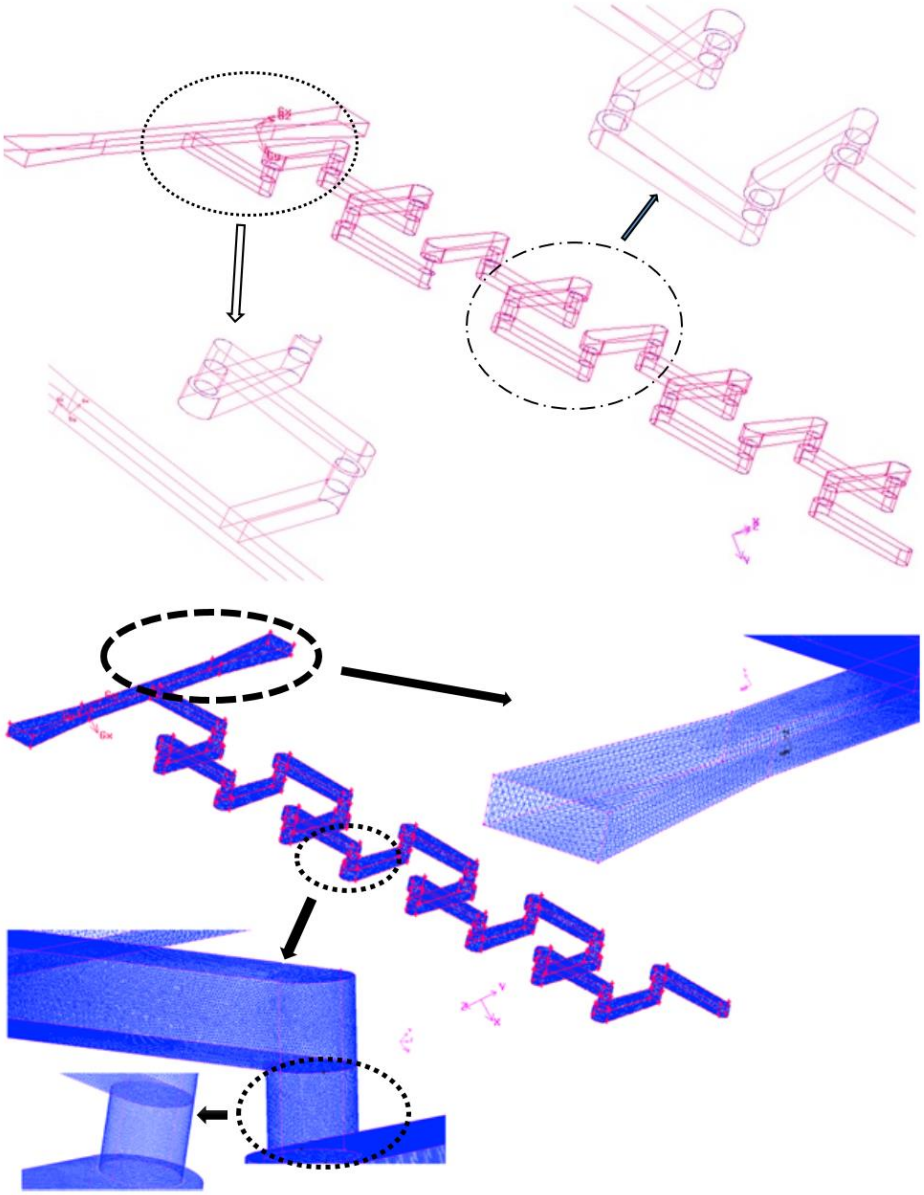

Fig 2. Geometry and its meshing

A high-quality mesh was necessary to avoid errors because of numerical diffusion. Therefore, mesh-independent solutions were checked for microchannel for different grids. So, to examine the independence of the results from the grid size, the variation of the pressure drop and Nusselt versus different nodes are shown in Fig 3. As it can be seen, the results of 150000 and 300000 grids are different from other grids (600000, 900000 and 1200000). Even though the 600000, 900000 and 1200,000 consequences are approximately the same, in order to lower computational cost, the 600,000 nodes have been opted.

a)

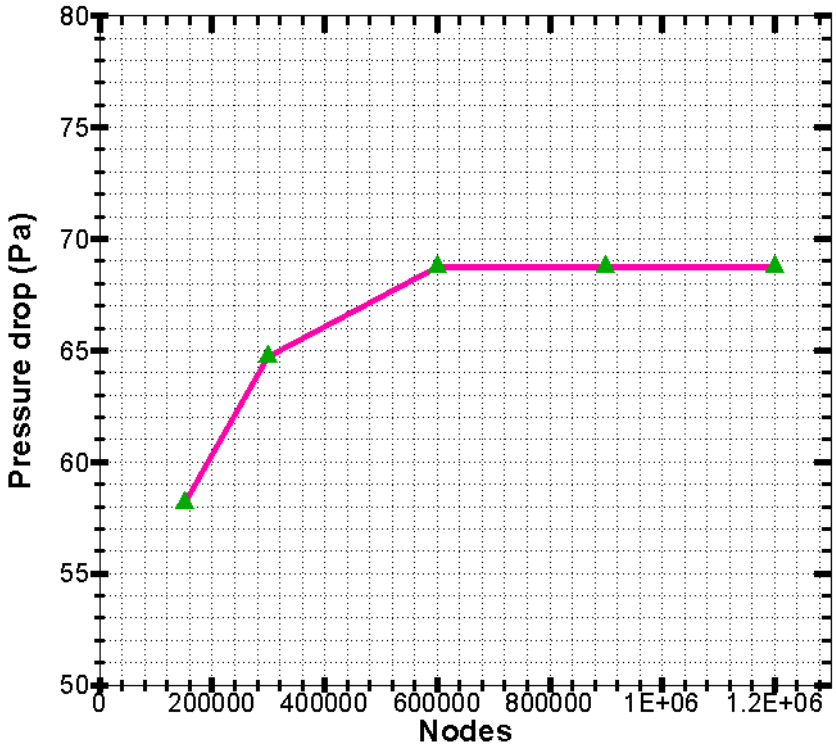

b)

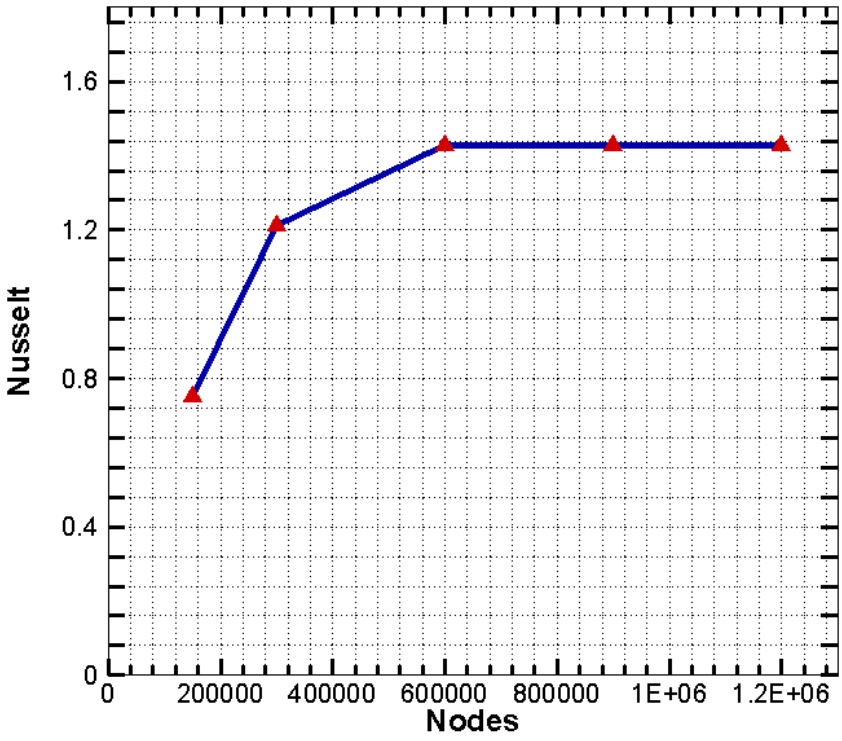

Fig 3. Grid independency for a) Pressure drop at Re= 4.166 and b) Nusselt for hybrid nano fluid when $\emptyset_{AL2O3} = \emptyset_{CuO} = \mathbf{0.5}$ % at Re=250

3.2 Model Validation

Figure 4. shows predicted variation of the pressure drop in comparison to the results of Victorov and Nimafar [70]Victorov and Nimafar investigated different types of micromixer including T, O, tear-drop and chain micromixers experimentally and numerically. In their experimental study, they used water as a fluid with different colors, so that the value of the ρ and μ were 998 ($kg\ m^{-3}$) and 0.000 89 ($kg\ m^{-1}s^{-1}$), respectively. Also some assumptions such as steady-state flow, no-slip conditions and incompressible fluid were proposed in their numerical part. In addition, experimental tests were performed using a microscope with high speed image acquisition. Colored waters were used as the mixing species in all tests; specifically, blue and yellow solutions were produced by blending 1g powder in 0.5lg water. Table 2 illustrates flow rate, Reynolds and velocity values during their experimental and numerical study. As it can be seen in Fig 4. good agreement was achieved between the experimental and the numerical results data taken from the studies by Victorov and Nimafar.

Table 2. Flow rate, Re and velocity values during experimental and numerical investigation of Victorov and Nimafar **[**70**]**

$Q_v(ml\ min^{-1})$	$Q_m(kg\ s^{-1})$	$V\ (mm\ s^{-1})$	Re
0.001	1.66×10^{-8}	0.1	0.083
0.005	8.31×10^{-8}	0.5	0.416
0.01	1.66×10^{-7}	1	0.832
0.02	3.32×10^{-7}	2	1.666
0.05	8.32×10^{-7}	5.2	4.166

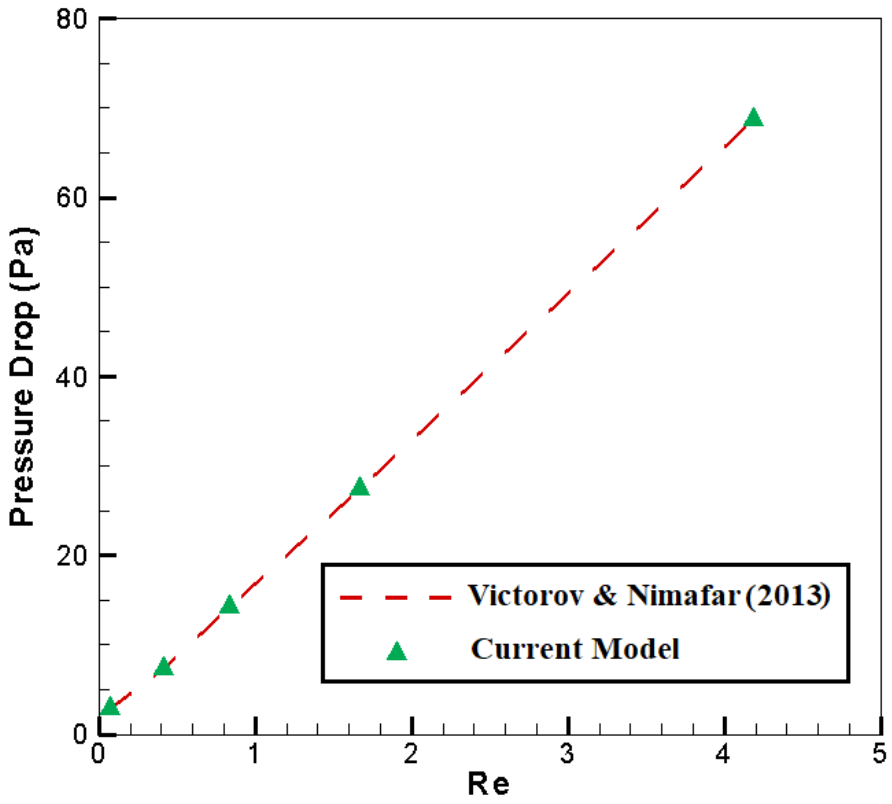

Fig 4. Pressure drop comparison of experimental and numerical model [61] and current simulation

4. Results and discussion

4.1 Effect of different types of nano fluids

The mushrooming developments of nanotechnology and thermal management techniques for enhancing cooling technology for electronic devices with high heat generation have made possible production of efficient and compact cooling modules to provide reliable system operation. In this section, the flow characteristics of various nanofluids with different nanoparticles has been investigated. Table 3 indicates thermo-physical properties of nanoparticles and nanofluids at $\emptyset_{Al_2O_3} = 4\%$ *and* $\emptyset_{CuO} = 4\%$.

Table 3 Thermo-physical properties of nanoparticles and nanofluids at $\emptyset_{Al_2O_3} = 4\%$ *and* $\emptyset_{CuO} = 4\%$

Material	Density, ρ $(\frac{kg}{m^3})$	Specific heat, C_p $(\frac{J}{kg.K})$	Thermal conductivity, k $(\frac{W}{m.K})$
CuO	6400	531	76.5
Al_2O_3	3600	765	36
Al_2O_3/Water	1086	3735.17	0.719

CuO/Water	1198	3407.5	0.721
Hybrid	1302.796	3091.74	0.8046

Figure 5 shows contour of static pressure for different nanofluids at Re= 416 when $\emptyset_{AL2O3} = \emptyset_{CuO} = \mathbf{4}$ %. It can be found that at Re=416, pressure drop for water is 48633 Pascal, whilst pressure drop for CuO-water, Al_2O_3-water and hybrid nanofluid have been faced with an increasing of 0.46%, 10.82% and 14.36% in comparison to poor water. At Re=416, there is considerable increase of pressure drop for Al_2O_3-water and hybrid nanofluid compared to poor water. The drawbacks of increasing pressure drop can not be addressed unless wide range of Reynolds number applies. To find the appropriate value for Reynold Number, the effect of Reynolds number on pressure drop for different nanofluid is illustrated in Fig 6. Having studied the data, it can be understood that pressure drop for water at Re= 0.416, 4.16, 41.6, 208 and 416 is 5.36, 55.03, 952.93, 13733.15 and 48633.13 Pascal, respectively, while CuO-water nanofluid has been associated with an augmentation of about 0.46% of pressure drop for aforementioned Reynolds numbers. In addition, pressure drop for Al_2O_3-water nanofluid at Re= 0.416, 4.16, 41.6, 208 and 416 is 5.94, 60.98, 1056.03, 15218.89, 53895.54 Pascal, respectively. Pressure drop for hybrid nanofluid has been accosted an increasing of about 3.3% in comparison to pressure drop of Al_2O_3-water nanofluid. So, in low Reynold number, the pressure drop will be decreased.

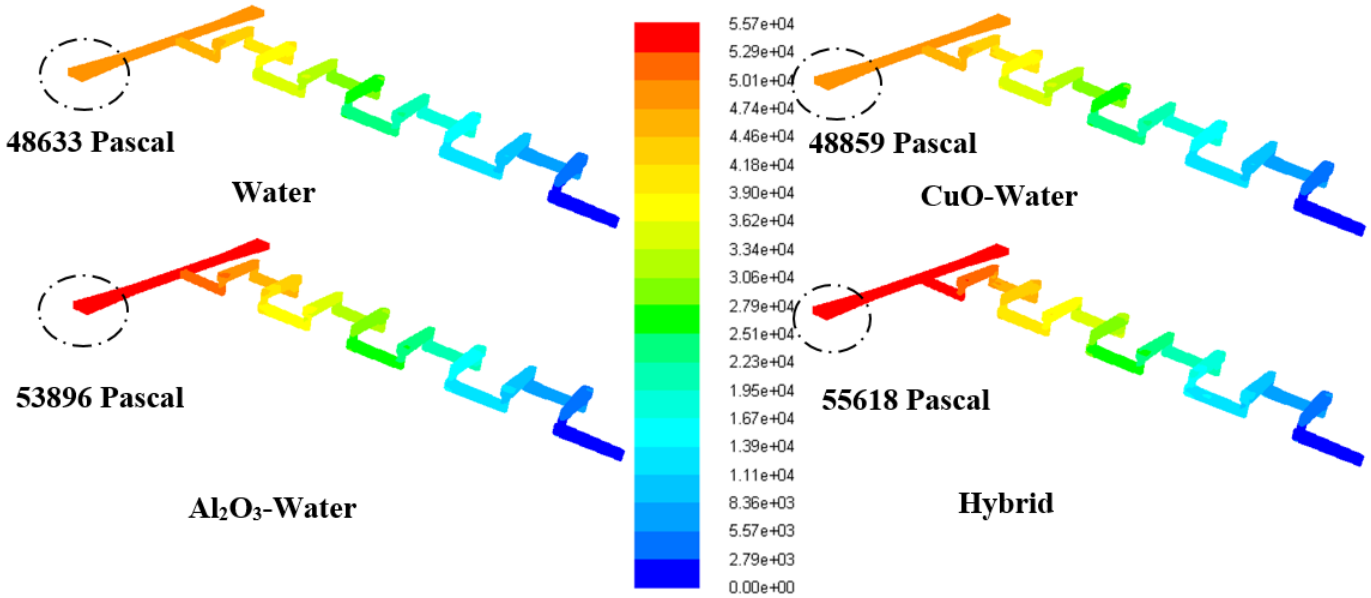

Fig 5. Contour of static pressure for different nanofluids at Re= 416 when $\emptyset_{AL2O3} = \emptyset_{CuO} = \mathbf{4}$ %

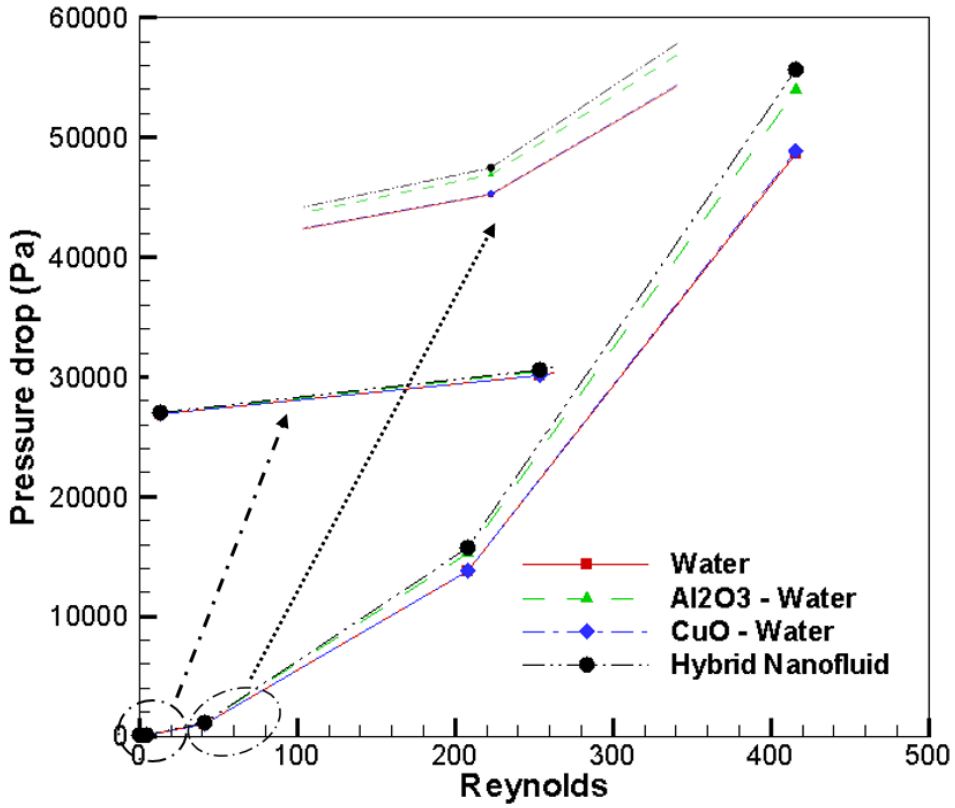

Fig 6. Pressure drop comparison at different Re for base fluid and different nano fluids when $\emptyset_{AL2O3} = \emptyset_{CuO} = \mathbf{4}$ %

4.2 Effect of nano fluid concentration

Nanofluids' thermal conductivity is an important thermo-physical property that determines their thermal efficiency. It is influenced by a number of parameters, including the concentration of nanoparticles, shape, size and thermal conductivity, stabilization methods, base fluid properties and thermal conductivity measurement techniques. In order to realize the trends of thermal conductivity of nanofluids, the individual or combined effects of these parameters are essential to consider. The thermal conductivity of nanofluids as a function of base fluid properties and nanoparticle concentration (φ) is summarized in this section. Thermo-physical properties of poor water and hybrid nanofluid has been calculated for different volumetric concentration and is shown in Table 4. The addition of nanoparticles enhances heat transfer by increasing the thermal conductivity of the base fluid, which optimizes the heat transfer capability and heat penetration of the fluid. This enhancement in heat transfer has been considered desirable from the standpoint of pure heat transfer, but it is undesirable since adding nanoparticles rises the viscosity and density of the base fluid, which result in increasing in pressure drop. This elucidates the need to investigate the effect of nanoparticles on the pressure drop. Figure 7 shows the pressure for hybrid nanofluid with different volume fraction at Re= 250. As can be seen, increasing volume fraction of nanoparticles, the pressure drop has also increased, so that pressure drop for poor water, $\emptyset_{AL2O3} =$

$\emptyset_{CuO} = 0.5, 1, 2, 3$ and 4 % is 19100, 19296, 19535, 20129, 20893 and 21883 Pascal. This is because by increasing the volume fraction of nanoparticles, the viscosity of the nanofluid increases. Therefore, the cohesion force between particles of the nanofluid increases leading to increase of pressure drops.

Table 4 Thermo-physical properties of water and hybrid nano fluid at different volume fraction

Type of Fluid	$\emptyset_{AL2O3}$ (%)	$\emptyset_{CuO}$ (%)	ρ $(\frac{kg}{m^3})$	C_p $(\frac{j}{kg.K})$	K $(\frac{w}{m.K})$	μ $(\frac{kg}{m.s})$
Water	-	-	981.3	4189	0.643	0.0006
Hybrid nano fluid	0.5	0.5	1021.487	4014.07	0.6618	0.0006153
	1	1	1061.487	3853.06	0.681	0.0006311
	2	2	1142.048	3563.15	0.721	0.0006645
	3	3	1222.422	3311.95	0.762	0.0007004
	4	4	1302.796	3091.74	0.8046	0.00074

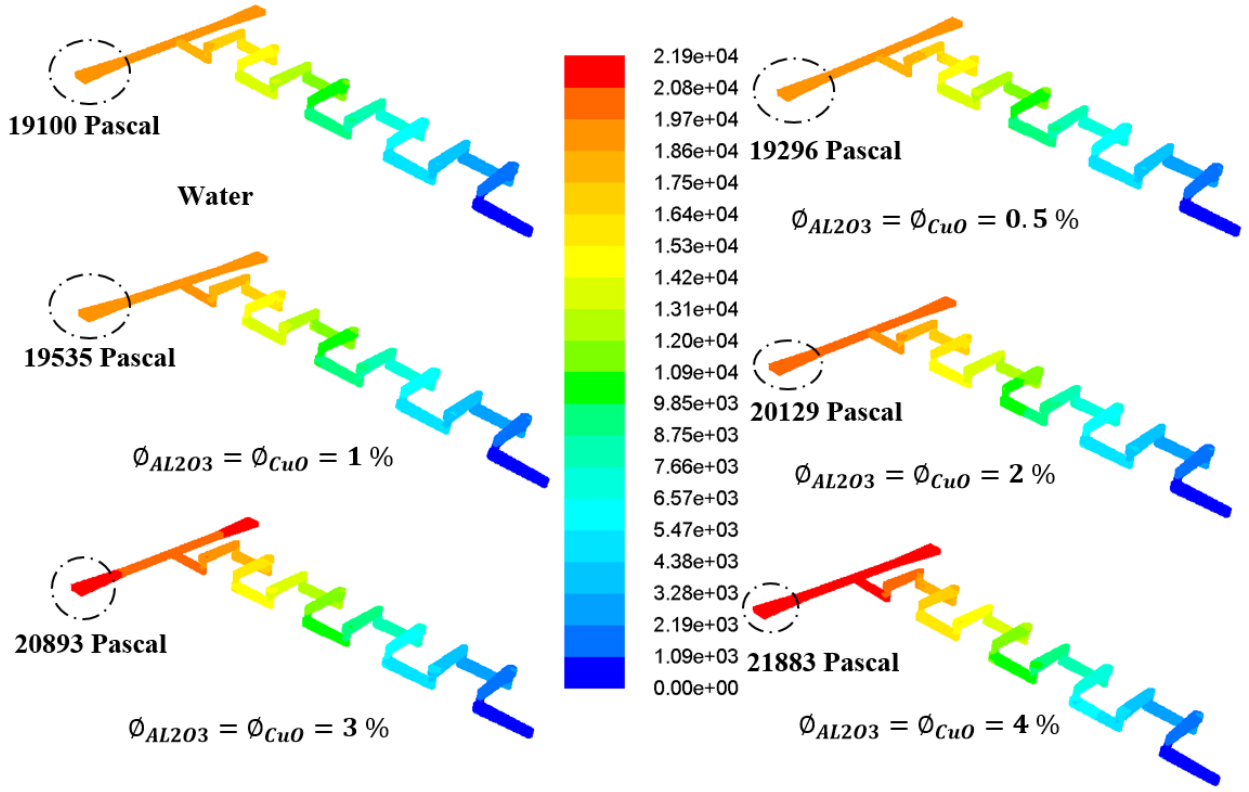

Fig 7. Contour of static pressure for hybrid nanofluid with different volume fraction at Re= 250

Figure 8 depicts the influences of Reynolds number and volume fraction of hybrid nanofluid on local Nusselt on Face1. It can be seen vividly that either augmenting Reynolds number from 125 up to 1000 or increasing volume fraction of hybrid nanofluid leads to rising trend of local Nusselt number. This subject matter can be enucleated by increasing the thermal conductivity through using different volume fraction of hybrid nanofluid with respect to water. Moreover, ρC_p of hybrid nanofluid compared to water amplifies; therefore more energy is required to enhance the bulk temperature with respect to water. So, the difference between bulk and wall temperature decreases in comparison to pure water, leading to growth in heat transfer characteristics. In addition, having studied the data from Fig 8, it can be considered that Nusselt for water at Re = 125, 250, 500 and 1000 is 0.98, 1.241, 1.664 and 2.18, respectively, whilst Nusselt for mentioned Reynolds numbers is 1.128, 1.427, 1.914 and 2.507, respectively when $\emptyset_{AL2O3} = \emptyset_{CuO} = 0.5\ \%$. Moreover, Nusselt number at aforementioned Reynolds numbers for $\emptyset_{AL2O3} = \emptyset_{CuO} = 4\ \%$ is 1.206, 1.541, 2.075 and 2.707,which, in turn, depicts surging of 22.94%, 24.17%, 24.70% and 24.707% in comparison to water, respectively. At Re=1000, the local Nusselt for $\emptyset_{\mathrm{AL2O3}} = \emptyset_{\mathrm{CuO}} = 1, 2, 3 \text{ and } 4\ \%$ is 2.557, 2.606, 2.655 and 2.707, which results in increasing of 1.99%, 3.95%, 5.9% and 7.98 compared to $\emptyset_{\mathrm{AL2O3}} = \emptyset_{\mathrm{CuO}} = 0.5\%$, respectively.

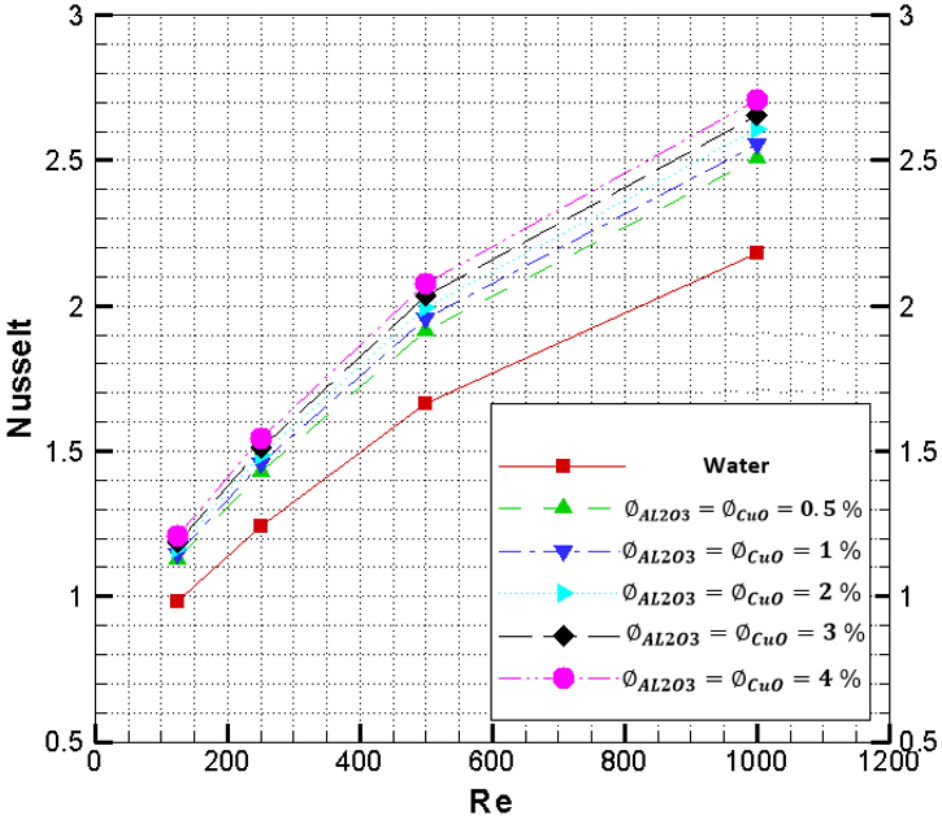

Fig 8. Nusselt versus Reynolds number for different volume fraction of hybrid nanofluid

4.3 Effect of electrode

Another approach to improve heat transfer performance is to use an electric field, which circulates and aligns the fluid towards the electrode. A graphical view of the computational domain has been depicted in Fig. 9. After validation of simulation with the geometry of Voctorov and Nimafar, the number of chains decreases. When the purpose of chain microchannel is to mix fluids, the number of chains in micromixer will be important. But, in this section, two chains have been considered due to obtaining results with better quality and taking into account the goal of this study is not to investigate mixing of fluids. The spot of emitter electrode is distinguished, whilst the plate electrode is fixed. The adjacent cells of the wire electrode and the walls of the microchannel are smaller, where it is expected more representative gradients will occur, as shown in Fig. 9b. To generate EHD flow, a configuration with discharge electrode and collector electrode (ground) were employed. A wire of 0.01 *mm* diameter was used as a discharge electrode. The emitter wire electrode is fixed at 7mm from the channel inlets. In addition, local Nusselt has been investigated on faces1 and 2, so that these faces are distinguished in Fig.9a.

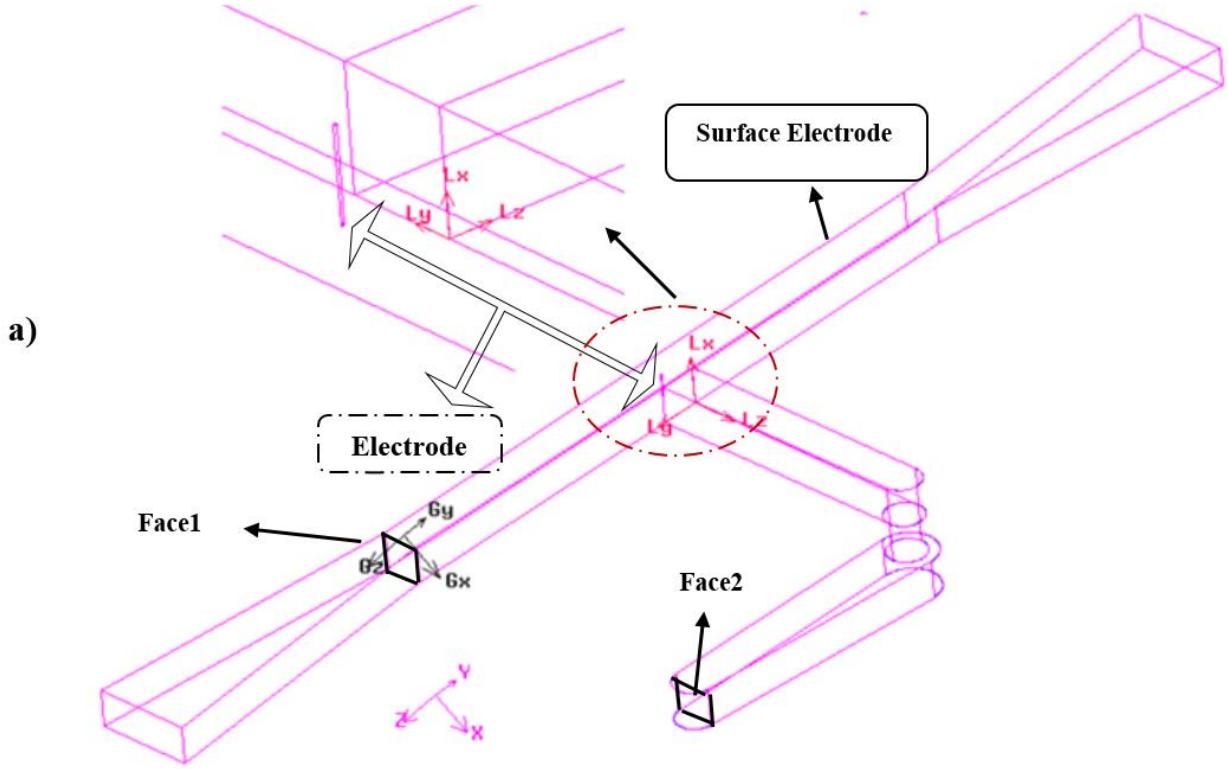

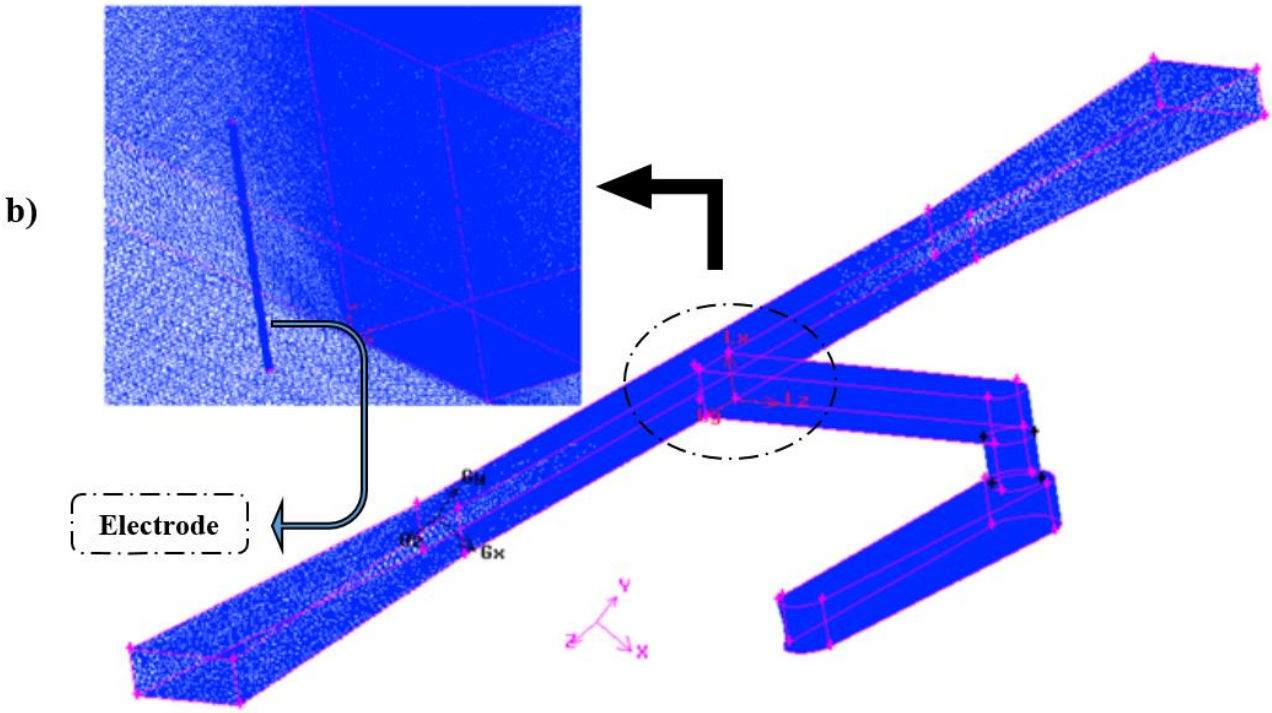

Fig 9. Electrode in chain microchannel, a) geometry, b) meshing

4.3.1 Effect of Hybrid Nano Fluid at low Reynolds

To obtain the desired performance, the shape of microchannels is an important design variable. The usage of chain microchannels as a micromixer is one of its applications and micromixers are important elements of microfluidic technology. The difficulty of mixing performance on the microscales depends on the small size of the micromixers. At high Reynolds numbers (typically > 2400), two fluids can easily be mixed by turbulence. It will be difficult to achieve in microchannel with less than one millimeter of cross-sections. The Reynolds numbers of liquids flowing through these microchannels are very small (typically <10). At a low Reynolds number, turbulent mixing does not happen and the solution is homogenized only through diffusion processes. At a low Reynolds number, flow in micromixers is intrinsically a diffusion-dominated laminar flow due to the microscale. Because of geometrical effects, it is evident that separating the layers of a mixture and recombining them results in quick mixing at low Reynolds numbers. A straight laminar flow arises when the Reynolds number is low, i.e. when there is no inertia in the flow. Even in bends, the path lines of flow follow the channel curvature as the number of flow layers and the contact surface area between the mixing fluids increases. Diffusion and convection are the basic mechanisms of fluid mixing in mixers. So, at the micro scale, molecular diffusion overcomes whilst convection is limited; consequently, mixing by diffusion at low Reynolds numbers needs too much time and a very long channel. Therefore, to accelerate the process, the contact area between the fluids to be mixed must be increased, and the fluids must be stretched, split and

recombined. Low energy requirements and high mixing efficiency are two keys characteristics of mixers. The cost of production would be reduced if the device's pressure drop was reduced. Mixing is ensured at low Reynolds numbers by generating multiple fluid lamellae. As the Reynolds number rises, vortexes emerge within the flow, eventually resulting in chaotic mixing. In fact, most micromixers can operate satisfactorily at either high or low Reynolds numbers – and chain micromixer has high energy requirements due to their complex structure. Therefore, the improvement of high-performance devices working in a wide range of Reynolds numbers with an acceptable pressure drop is presently a major focus of this section. Figures 10 and 11 illustrated the counter of pressure for poor water and hybrid nanofluid at low Reynolds number ($0.416 \leq Re \leq 4.166$). Pressure drop for poor water at Re = 0.416, 1.666, 2.499 and 4.166 is 1.05, 4.16, 6.25 and 10.45 Pascal, respectively, whilst it has been obtained 1.18, 4.75, 7.15 and 12 Pascal for hybrid nanofluid at aforementioned Reynolds, respectively. On the other word, using hybrid nanofluid, in aforementioned Reynolds number, leads to increase of 12.38%, 14.18%, 14.40% and 14.83% of pressure drop, respectively. It can be found that at low Reynolds range, the lower Reynolds results in decreasing of percentage of pressure drop.

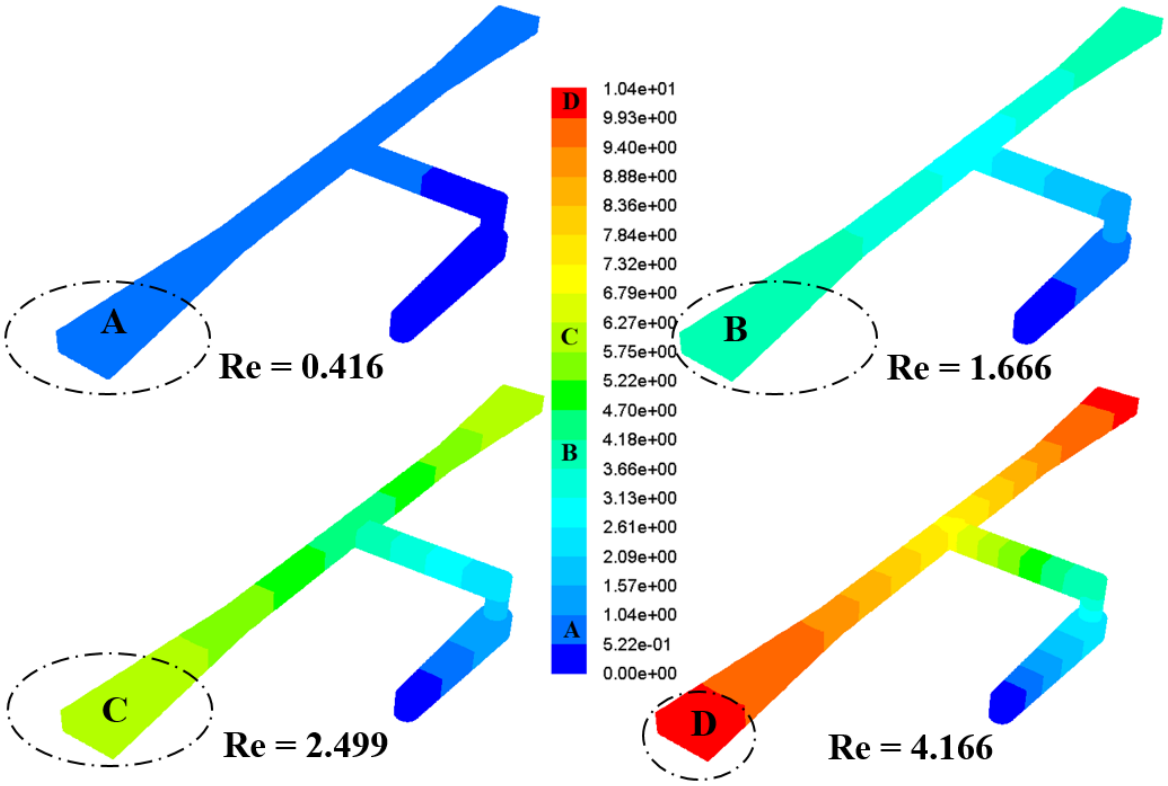

Fig 10. Static Pressure (Pascal) for different Re for water

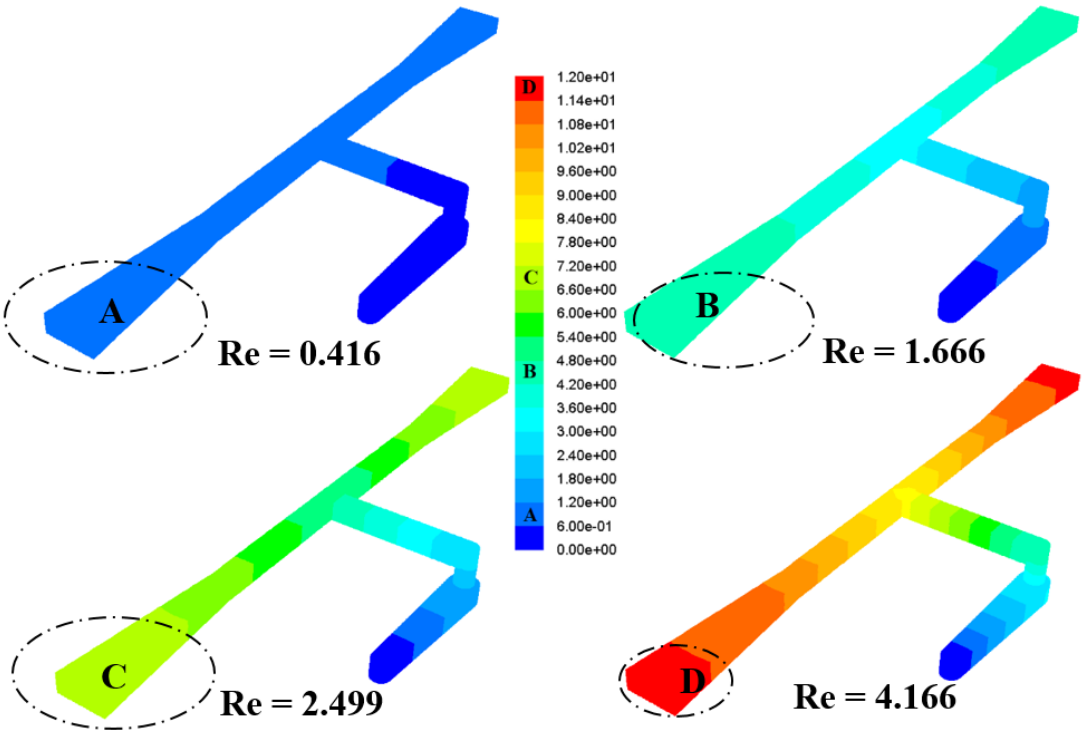

Fig 11. Static pressure (Pascal) for different Re for hybrid nano fluid when $\emptyset_{AL2O3} = \emptyset_{CuO} = \mathbf{4}$ %

4.3.2 Effect of EHD

The enhancing impact of strong electric field (EHD enhancement) on heat transfer rate has been very well known over many decades. Most of the research was focused on single-phase flows, but in recent years, EHD has proven to be very useful in improving heat transfer in two-phase flows. Keeping this discussion mind, the main goal of present paper is to simulate the impact of Coulomb forces on hybrid nanofluid hydrothermal treatment. Figures 12 and 13 depict the results of the electric potential and charge density. The figures illustrate that there were applied electric potentials at the surface of the discharge wire. Also, the charges were transported from the discharge wire along the electric field, which was formed by the divergence of electric potential. It is clear that the electrical potential and charge becomes stronger near the emitters.

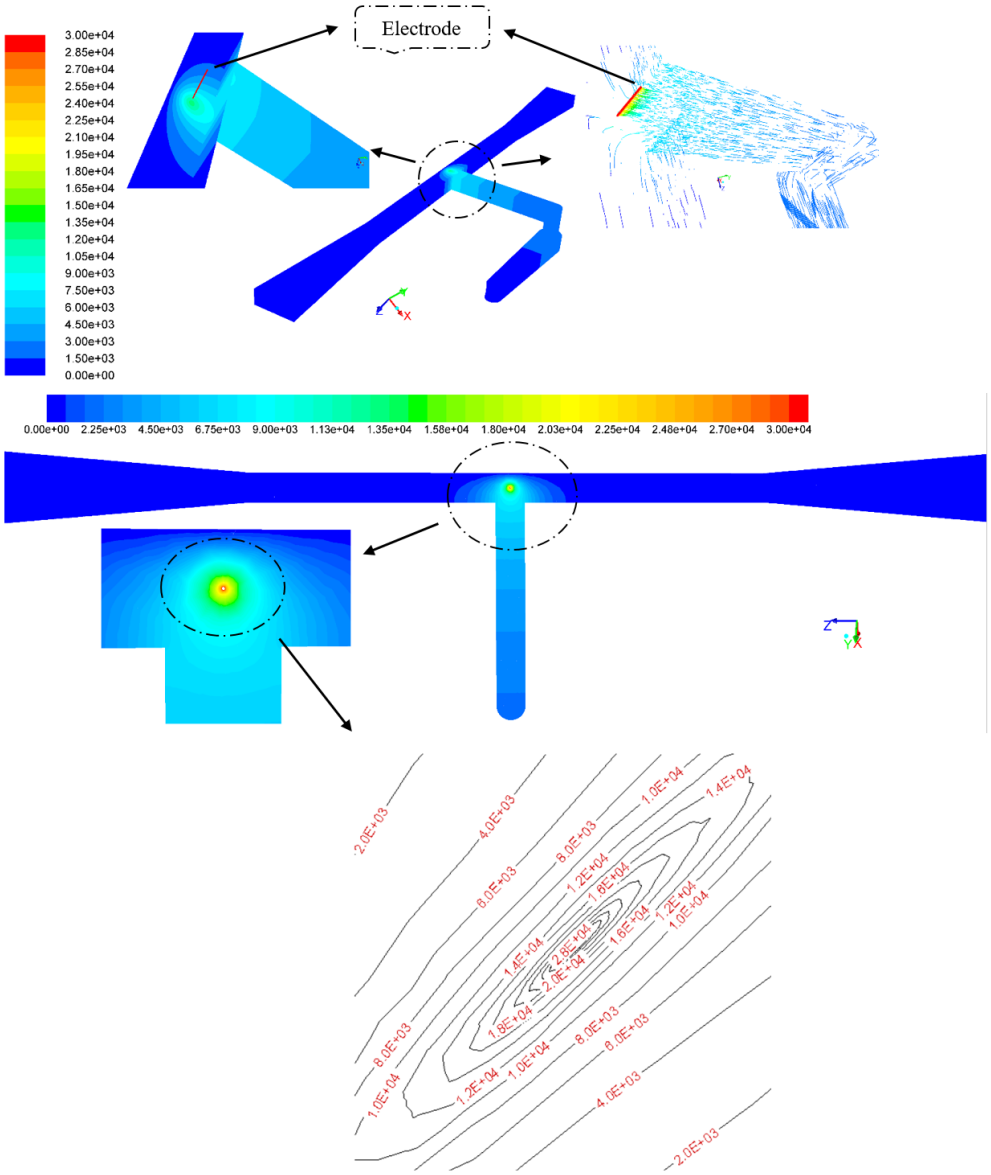

Fig 12. Electrical potential contour at voltage 30 KV

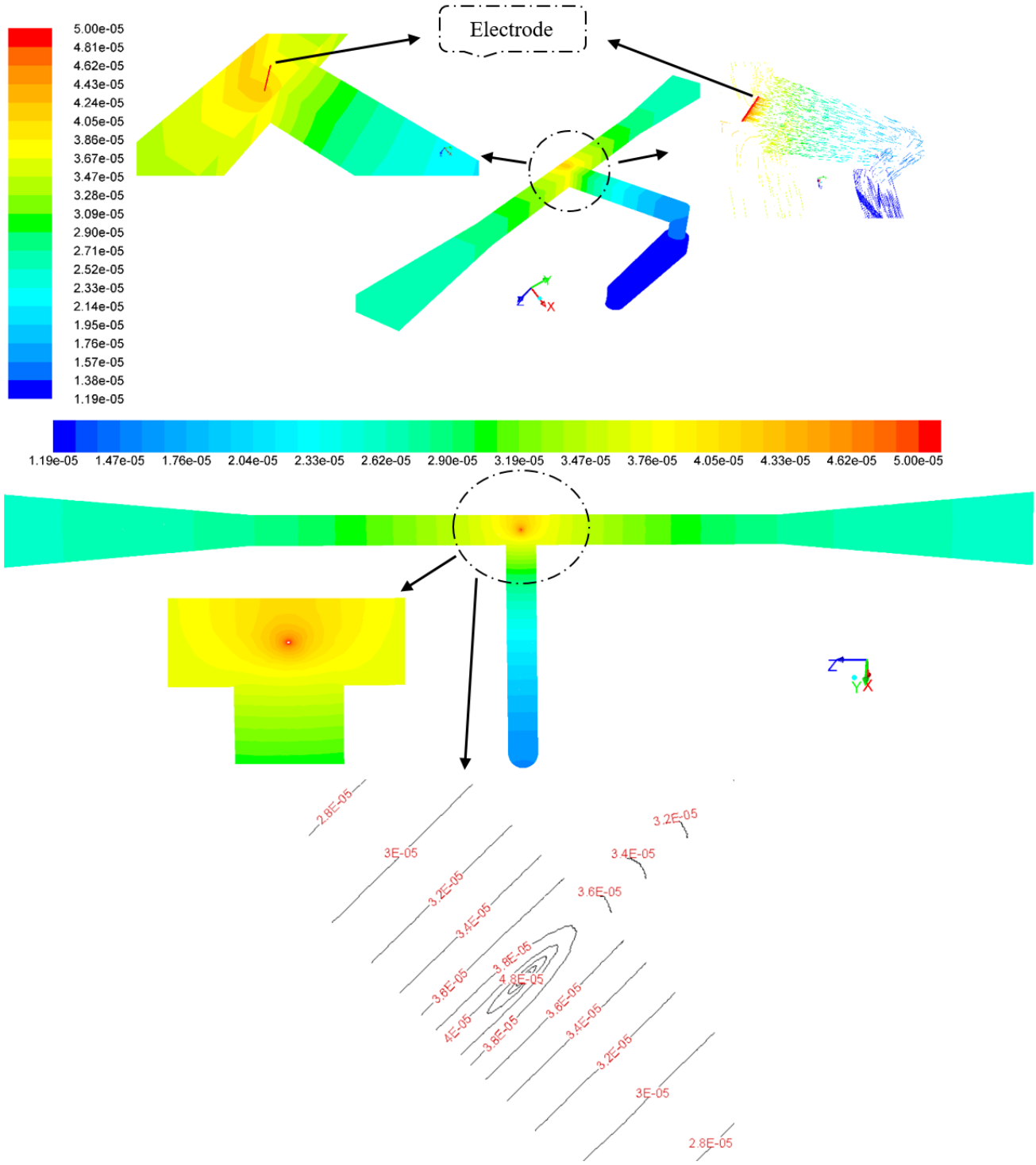

Fig 13. Electric charge contour at voltage 30 KV

To investigate the effect of using EHD, heat transfer enhancement and distribution of pressure drop should be considered together. Figure 14 depicts contour of pressure in the presence and absence of electrical field. Results show that pressure drop for non-use of EHD and using EHD is 12 Pascal and 21.3 Pascal at Re=4.166. So, the drawbacks of increasing pressure drop in the presence of electric field should be noted.

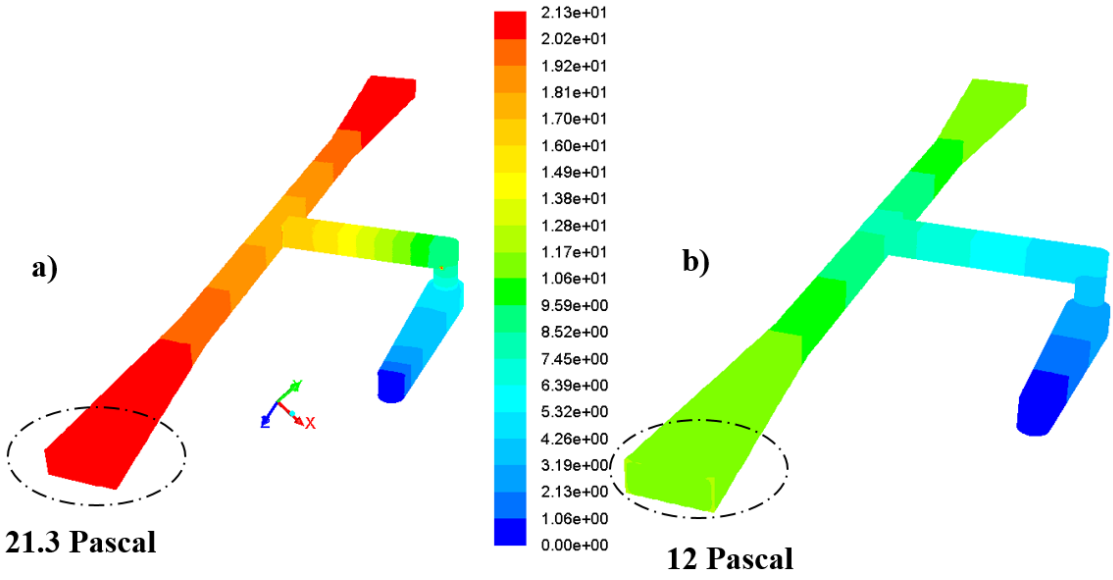

Fig 14. Contour of static pressure at Re= 4.166 when $\emptyset_{AL2O3} = \emptyset_{CuO} = \mathbf{4}$ %, a) with EHD at 30 KV, b) without EHD

Local Nusselt number for faces 1 and 2 (Fig 9a) are defined as follows:

$$Nu = \frac{hd}{k_f} = \frac{q''.d}{k_f.(T_{bulk} - T_{wall})} \tag{23}$$

Where d is the characteristic length and k_f is thermal conductivity depends of used nanofluid. In Fluent, q'' and T_{bulk} will be obtained from area-weighted average and mass-weighted average, respectively.

Figures 15 and 16 show local Nusselt number versus Reynolds number for faces 1 and 2. For face1, it can be seen that in the absence of electrical field, the Nusselt for Re= 125, 250, 500 and 1000 is 1.1, 1.4, 1.77 and 2.25, respectively, while Nusselt in the presence of voltage 30 (KV) for aforementioned Reynolds number is 1.353, 1.708, 2.124 and 2.655, respectively. On the other word, imposing voltage (30 KV) leads to increasing of 23%, 22%, 20% and 18% of Nusselt number, respectively. It denotes that rising the Nusselt number in lower Reynolds number is more efficient.

For face 2, Nusselt number is 0.74, 0.84, 1.18 and 1.56 for aforementioned Reynolds numbers, so that it has been faced with augment of 20%, 18%, 17% and 16%, respectively, in the presence of 30 KV voltage. These observations confirm that the impact of electric field is more marked for lower Reynolds number.

Figure 17 demonstrates average Nusselt number versus Reynolds number when $\emptyset_{AL2O3} = \emptyset_{CuO} =$ **4** % and V= 30 KV. Average Nusselt number without electrical field is 0.95, 1.15, 1.505 and 1.935 for aforesaid Reynolds number, respectively, whilst average Nusselt number is 1.1605, 1.3896, 1.7923 and 2.2723 for above-mentioned Reynolds number, respectively. To more elaborate, a strong rotating vortex results from the presence of EHD induced flow, which, in turn, causes quick mixing between the core and wall flow especially at low Reynolds number.

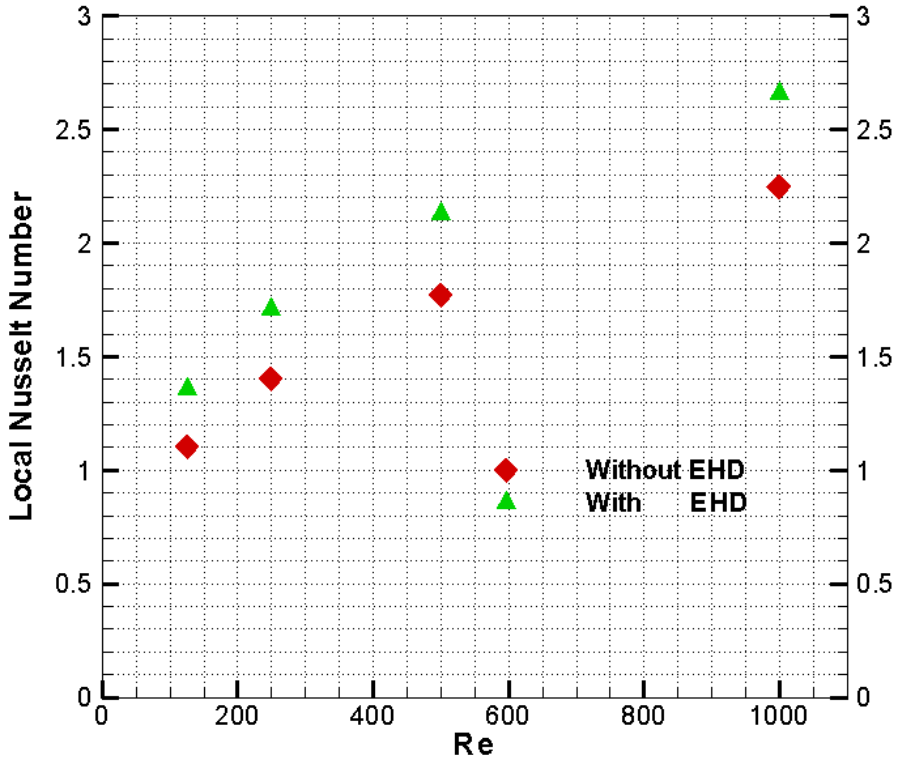

Fig 15. Local Nusselt number versus Re when $\emptyset_{AL2O3} = \emptyset_{CuO} =$ **4** % and V= 30 KV at Face1

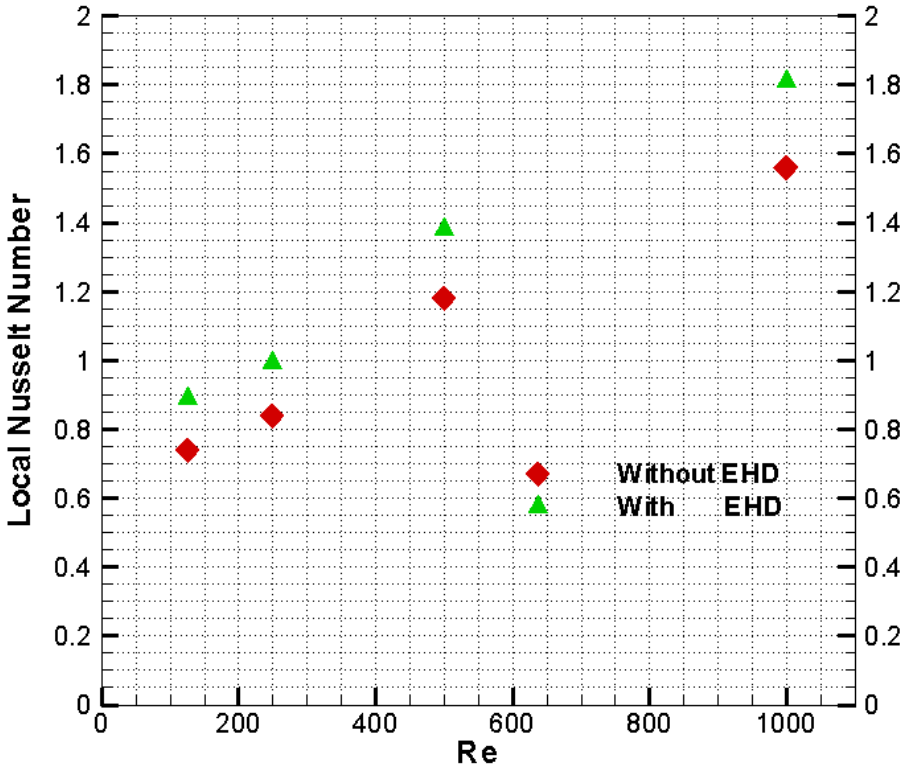

Fig 16. Local Nusselt number versus Re when $\emptyset_{AL2O3} = \emptyset_{CuO} = \mathbf{4}$ % and V= 30 KV at Face2

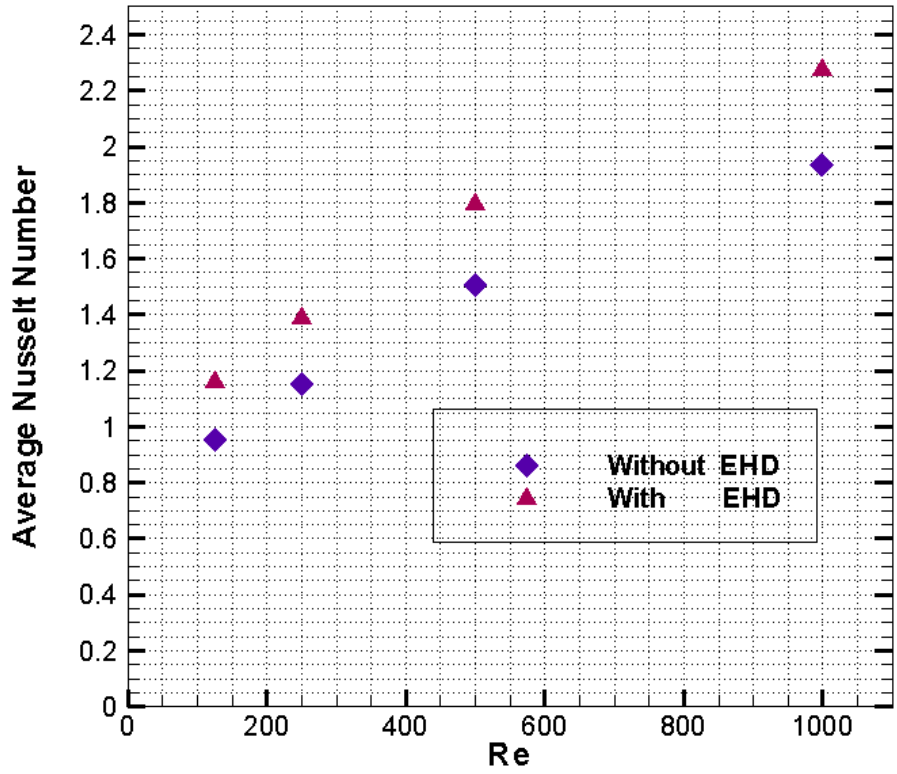

Fig 17. Average Nusselt number versus Re when $\emptyset_{AL2O3} = \emptyset_{CuO} = \mathbf{4}$ % and V= 30 KV

4.3.3 Effect of different voltages

As the voltage has been increased, the ions move faster because of the higher intensity of the electric field, leads to more ionization and collision. In addition, faster ions have larger momentum, leads to drag the fluid particles, which, in turn, causes higher heat transfer enhancement. Moreover, in Low-Reynolds number cases (laminar flow), the ions are more efficacious in conveying momentum to slow-moving particles. However, as the fluid momentum rises with Reynolds number, the ions' ability to generate secondary motion and extra momentum reduces, so the level of enhancement is decreased. The enhancement provided by corona wind in Low-Reynolds (laminar) flows is now much more pronounced. This means that, the corona wind is not only overshadowed by turbulence, but also it is less effective at higher values of Re. Increasing of Reynolds number resulting in rising Nusselt number because of a decrease in thermal boundary layer thickness. Increasing supplied voltage causes the isotherms more distorted. Higher values of applied voltage leads to maximize the local Nusselt number owing to presence of thermal plumes. Nusselt number is a rising function of applied voltage. In the absence of electric field, Nusselt number for face1 at Re = 125, 250, 500 and 1000 is 1.1, 1.4, 1.77 and 2.25. Having perused the data from Fig. 18 for Re=125, 250, 500 and 1000, it can be understood that at the voltage of 10 (KV), Nusselt number has been faced with an increasing of 16.82%, 15.93%, 14.01% and 12.09%, respectively, whilst this rising is 19.27%, 18.36%, 17% and 14.44% in comparison to absence of electrical field. Moreover, nusselt increased 23%, 22%, 20% and 18% at 30 (KV) and 25.45%, 24.43%, 22.37% and 20.36% for aforementioned Reynolds number, respectively, compared to non-use of electrical field.

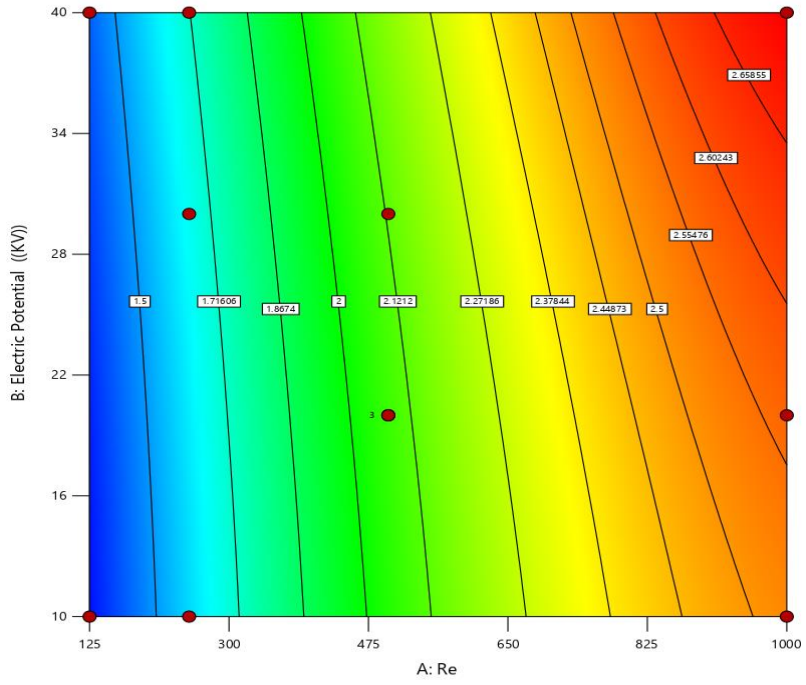

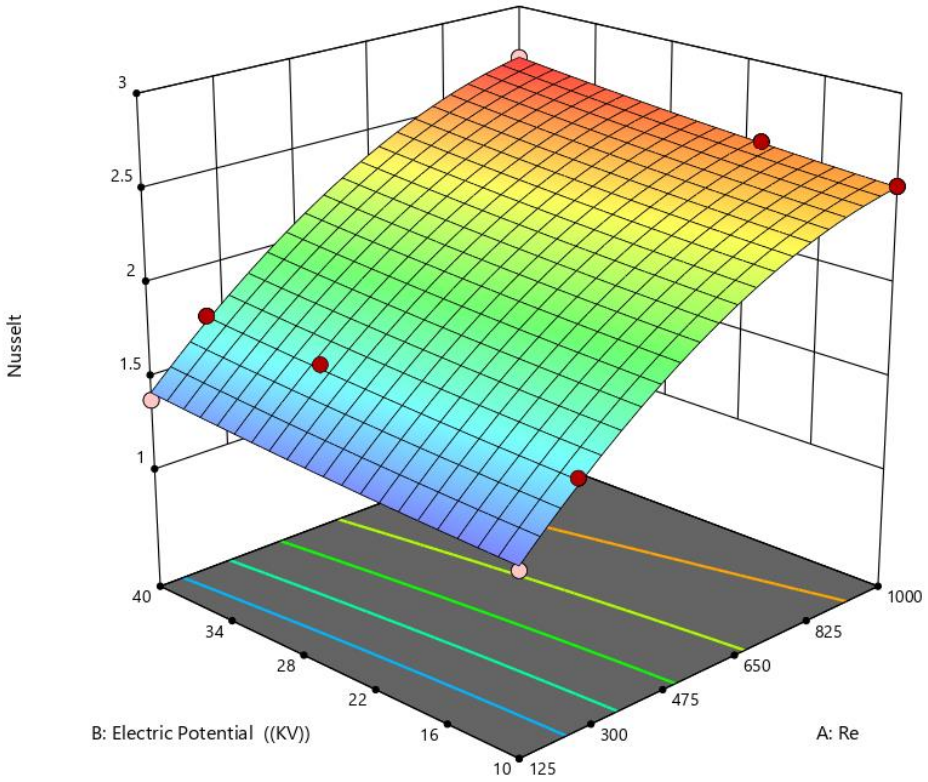

Fig 18. Effects of Reynolds number and applied voltages on local Nusselt number at face1 when $\emptyset_{AL2O3} = \emptyset_{CuO} =$ **4** %

For face 2, at V=10 (KV) for Re=125, 250, 500 and 1000, Nusselt number raised 14%, 12.10%, 11.19% and 10.26%, at 20 (KV), it shows increasing of 16.41%, 14.46%, 13.56% and 12.56% in comparison to 0 (KV). In addition, increasing of 20%, 18%, 17% and 16% have been obtained at 30 (KV), and, for 40 (KV), this values are 22.41%, 20.36%, 19.49% and 18.59%, respectively, compared to non-use of electrical filed. So, the enhancement caused by corona wind in lower-Re flows is now much more pronounced.

Figure 20 displays the effects of Reynolds number and applied voltages on average Nusselt number when $\emptyset_{AL2O3} = \emptyset_{CuO}$=4 %. It can be seen that average Nusselt number at 10 (KV) is 1.0943, 1.3223, 1.695 and 2.151, while it is 1.1729, 1.4065, 1.818 and 2.3091 at 40 (KV) for forenamed Reynolds number.

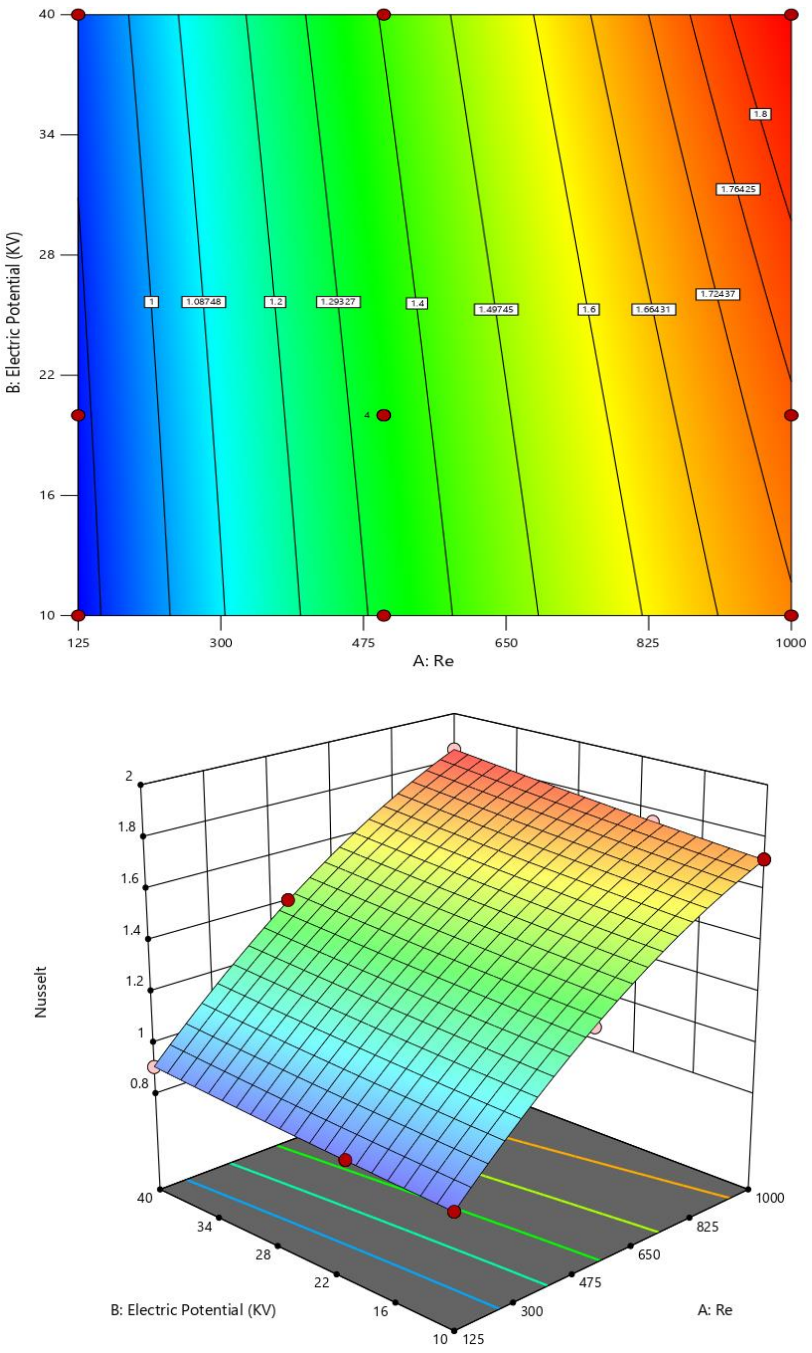

Fig 19. Effects of Reynolds number and applied voltages on local Nusselt number at face2 when $\emptyset_{AL2O3} = \emptyset_{CuO}$

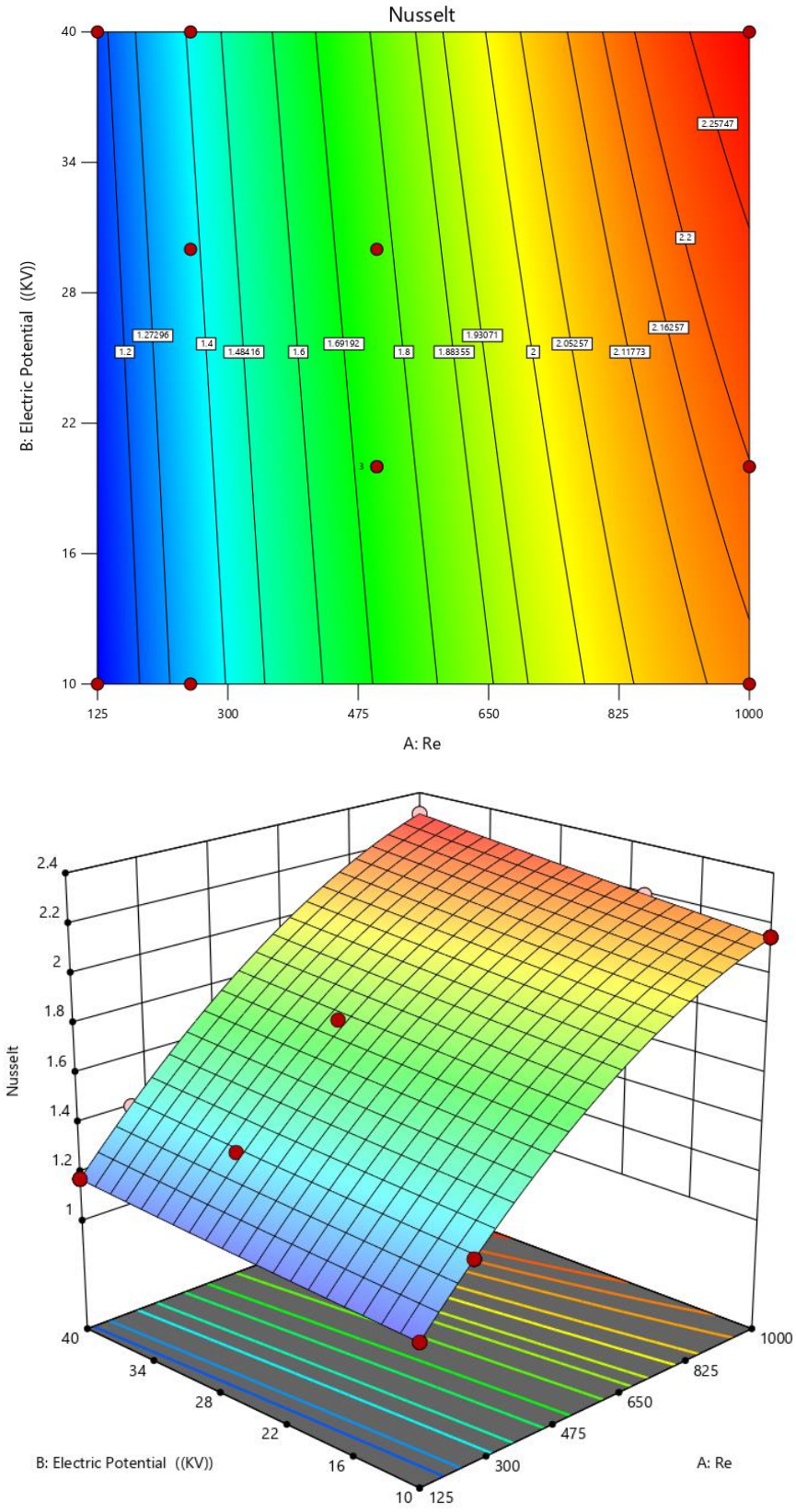

Fig 20. Effects of Reynolds number and applied voltages on average Nusselt number when $\emptyset_{AL2O3} = \emptyset_{CuO}$=4 %

5. Conclusion

In this work, a nanofluid-based chain microchannel integrated with EHD using a steady, laminar and three-dimensional model was numerically simulated. Thermo-physical properties of nanofluid and hybrid nanofluid were applied to predict the behavior of the system. Al_2O_3 and CUO nanoparticles were dispersed into working fluid to improve their thermal behavior. To optimize the chain microchannel using nanofluids, effect of nano fluid concentration was analyzed. Eventually, this nanofluid-based chain microchannel system integrated with EHD was optimized regarding hybrid nanofluid at low Reynolds according to selecting different voltages for the proposed system performance. Results indicate that the influence of Coulomb force is more useful for low values of Reynolds number. Results also show that by increasing the volume fraction of nanoparticles, the viscosity of the nanofluid increases leading to an increase in pressure drops. Meanwhile, imposing electrohydrodynamic force leads to increasing the Nusselt number in comparison to absence of electric field. It means that the considered effect of the increasing the Nusselt number at lower Reynolds number is more effective. Moreover, heat transfer rises with augmentation of supplied voltage and Reynolds number.

The details of contributed results can be summarized as follow:

- Lowest increasing of pressure drop belongs to CuO-water at Re=416, so that pressure drop for CuO-water, Al_2O_3-water and hybrid nanofluid have been faced with rising of 0.46%, 10.82% and 14.36% in comparison to poor water.
- Pressure drop for hybrid nanofluid has been accosted an increasing of about 3.3% in comparison to pressure drop of Al_2O_3- water nanofluid.
- Increasing volume fraction of nanoparticles leads to rising the pressure drop.
- Nusselt at Re = 125, 250, 500 and 1000 for hybrid nanofluid ($\emptyset_{AL2O3} = \emptyset_{CuO} = 4\ \%$) is 1.206, 1.541, 2.075 and 2.707,which, in turn, depicts surging of 22.94%, 24.17%, 24.70% and 24.707% in comparison to poor water, respectively.
- At Re=1000, local Nusslet for $\emptyset_{\mathrm{AL2O3}} = \emptyset_{\mathrm{CuO}} = 1, 2, 3$ and 4 % is 2.557, 2.606, 2.655 and 2.707, which results in increasing of 1.99%, 3.95%, 5.9% and 7.98 compared to $\emptyset_{\mathrm{AL2O3}} = \emptyset_{\mathrm{CuO}} = 0.5\%$, respectively.
- At Re = 0.416, 1.666, 2.499 and 4.166, using hybrid nanofluid leads to increase of 12.38%, 14.18%, 14.40% and 14.83% of pressure drop, respectively. In other words, the lower Reynolds results in decreasing of percentage of pressure drop.
- For face 1, imposing EHD (V=30 KV) leads to increasing of 23%, 22%, 20% and 18% of Nusselt number compared to the absence of electrical filed, respectively.
- For face 2, Nusselt number is 0.74, 0.84, 1.18 and 1.56 for aforementioned Reynolds number, so that it has been faced with augment of 20%, 18%, 17% and 16%, respectively, in the presence of 30 KV of voltage.

- At the voltage of 10 (KV), Nusselt number has been faced with an increasing of 16.82%, 15.93%, 14.01% and 12.09%, respectively, whilst this rising is 19.27%, 18.36%, 17% and 14.44% in comparison to absence of electrical field.
- Nusselt increased 23%, 22%, 20% and 18% at 30 (KV) and 25.45%, 24.43%, 22.37% and 20.36% for aforementioned Reynolds number, respectively, compared to non-use of electrical field.
- For face 2, at V=10 (KV) for Re=125, 250, 500 and 1000, Nusselt number raised 14%, 12.10%, 11.19% and 10.26%.
- At 20 (KV), it has been faced with an increasing of 16.41%, 14.46%, 13.56% and 12.56% in comparison to 0 (KV).
- Increasing of 20%, 18%, 17% and 16% have been obtained at 30 (KV), and, for 40 (KV), this values are 22.41%, 20.36%, 19.49% and 18.59%, respectively, compared to non-use of electrical filed.
- The enhancement caused by corona wind in lower-Re flows is now much more pronounced.

CRediT author statement

Milad Amiri: Conceptualization; Methodology; Data curation; Formal analysis; Funding acquisition; Investigation; Project administration; Resources; Software; Validation; Visualization; Writing - original draft; Writing - review & editing.

Dariusz Mikielewicz: Conceptualization; supervision; project administration; funding acquisition

Nomenclature			
C_p	Specific heat capacity ($J.kg^{-1}K^{-1}$)	***Greek Symbols***	
$\vec{E}$	Electric field strength vector (V/s)	ρ_c	Charge density (C/m^3)
j	Electric current density (A/m^2)	ρ	Density (kg/m^3)
k	Thermal conductivity coefficient	$\emptyset$	Overall volume concentration
T	Temperature (^0C)	$\emptyset_s$	Volume fraction of particles
$\vec{u}$	Velocity vector (m/s)	β	Ion mobility ($m^2/(V \cdot s)$)
V	Electric potential (V)	μ	Dynamic viscosity ($kg.m^{-1}.s^{-1}$)
Subscript		S_{ζ_k}	Source term
n	Nano fluid	Γ_k	Diffusion coefficient
hnf	Hybrid Nano fluid		

Declaration of interests

☒ The authors declare that they have no known competing financial interests or personal relationships that could have appeared to influence the work reported in this paper.

☐The authors declare the following financial interests/personal relationships which may be considered as potential competing interests:

References:

[1] M. Sheikholeslami and M. Bhatti, "Active method for nanofluid heat transfer enhancement by means of EHD," *International Journal of Heat and Mass Transfer,* vol. 109, pp. 115-122, 2017. https://doi.org/10.1016/j.ijheatmasstransfer.2017.01.115.

[2] V. Ganapathy, *Steam generators and waste heat boilers: for process and plant engineers*. CRC Press, 2014.

[3] P. Ziółkowski *et al.*, "Thermodynamic analysis of negative CO2 emission power plant using Aspen Plus, Aspen Hysys, and Ebsilon software," *Energies,* vol. 14, no. 19, p. 6304, 2021. https://doi.org/10.3390/en14196304.

[4] P. Ziółkowski *et al.*, "Mathematical modelling of gasification process of sewage sludge in reactor of negative CO2 emission power plant," *Energy,* vol. 244, p. 122601, 2022. https://doi.org/10.1016/j.energy.2021.122601.

[5] P. Ziółkowski, K. Stasiak, M. Amiri, and D. Mikielewicz, "Negative carbon dioxide gas power plant integrated with gasification of sewage sludge," *Energy,* p. 125496, 2022. https://doi.org/10.1016/j.energy.2022.125496.

[6] D. Mikielewicz, M. Amiri, and J. Mikielewicz, "A Simple Analytical Model of Direct-Contact Condensation from Vapour-Inert Gas Mixture in a Spray Ejector Condenser," *Available at SSRN 41*.47312.2022. http://dx.doi.org/10.2139/ssrn.4147312.

[7] D. Mikielewicz, M. Amiri, and J. Mikielewicz, "Direct-contact condensation from vapour-gas mixture in a spray ejector condenser for negative CO2 power plant," 2022. https://mostwiedzy.pl/pl/publication/direct-contact-condensation-from-vapour-gas-mixture-in-a-spray-ejector-condenser-for-negative-co2-po,158333-1

[8] A. Šalić, A. Tušek, and B. Zelić, "Application of microreactors in medicine and biomedicine," *Journal of Applied Biomedicine,* vol. 10, no. 3, pp. 137-153, 2012. https://doi.org/10.2478/v10136-012-0011-1.

[9] J. Bassols, B. Kuckelkorn, J. Langreck, R. Schneider, and H. Veelken, "Trigeneration in the food industry," *Applied Thermal Engineering,* vol. 22, no. 6, pp. 595-60 .2002. https://doi.org/10.1016/S1359-4311(01)00111-9.

[10] A. Ameen, *Refrigeration and air conditioning*. PHI Learning Pvt. Ltd., 2006.

[11] C. Chen, D. Buddhi, A. Sharma, V. Tyagi, C. Chen, and D. Buddhi, "Review on thermal energy storage with phase change material and applications," *Renew. Sustain. Energy Rev,* vol. 13, pp. 318-345, 2009. https://doi.org/10.1016/j.rser.2007.10.005.

[12] D. R. Heldman and C. I. Moraru, *Encyclopedia of agricultural, food, and biological engineering*. Crc Press, 2010.

[13] C. Oliet, A. Oliva, J. Castro, and C. Perez-Segarra, "Parametric studies on automotive radiators," *Applied thermal engineering,* vol. 27, no. 11-12, pp. 2033-2043, 2007. https://doi.org/10.1016/j.applthermaleng.2006.12.006.

[14] T. A. Ring, *Fundamentals of ceramic powder processing and synthesis*. Elsevier, 1996.

[15] J. Beddoes and M. Bibby, *Principles of metal manufacturing processes*. Butterworth-Heinemann, 1999.

[16] A. K. Coker, *Petroleum Refining Design and Applications Handbook*. John Wiley & Sons, 2018.

[17] P. Mitchell, *Tool and manufacturing engineers handbook: plastic part manufacturing*. Society of Manufacturing Engineers, 1996.

[18] P. Bajpai, *Pulp and paper industry: energy conservation*. Elsevier, 2016.

[19] A. A. Minea, "Hybrid nanofluids based on Al2O3, TiO2 and SiO2: numerical evaluation of different approaches," *International Journal of Heat and Mass Transfer,* vol. 104, pp. 852-860, 2017. https://doi.org/10.1016/j.ijheatmasstransfer.2016.09.012

[20] E. M. Abo-Zahhad *et al.*, "Four compartments stepwise varied width microchannels cooling approach for densely-packed module of concentration photovoltaics," in *International Conference*

on Nanochannels, Microchannels, and Minichannels, 2020, vol. 83 :693American Society of Mechanical Engineers, p. V001T04A002. https://doi.org/10.1115/ICNMM2020-1006

[21] A. Y. M. Ali, A. H. El-Shazly, M. F. El-Kady, H. I. Elqady, and M. R. El-Marghany, "Effect of using MgO-oil nanofluid on the performance of a counter-flow double pipe heat exchanger," in *Key Engineering Materials*, 2019, vol. 801: Trans Tech Publ, pp. 193-198. https://doi.org/10.4028/www.scientific.net/KEM.801.193

[22] H. Mario Di Capua, R. Escobar, A. Diaz, and A. M. Guzmán, "Enhancement of the cooling capability of a high concentration photovoltaic system using microchannels with forward triangular ribs on sidewalls," *Applied Energy*, vol. 226, pp. 160-180, 2018. https://doi.org/10.1016/j.apenergy.2018.05.052.

[23] M. H. Mousa, N. Miljkovic, and K. Nawaz, "Review of heat transfer enhancement techniques for single phase flows," *Renewable and Sustainable Energy Reviews*, vol. 137, p. 110566.2021 , https://doi.org/10.1016/j.rser.2020.110566.

[24] N. Kasayapanand, J. Tiansuwan, W. Asvapoositkul, N. Vorayos, and T. Kiatsiriroat, "Effect of the electrode arrangements in a tube bank on the characteristic of electrohydrodynamic heat transfer enhancement: low reynolds number," *Journal of Enhanced Heat Transfer*, vol. 9, no. 5-6, pp. 229-242, 2002. DOI: 10.1080/10655130216024.

[25] M. Sheikholeslami, S. Soleimani, and D. Ganji, "Effect of electric field on hydrothermal behavior of nanofluid in a complex geometry," *Journal of Molecular Liquids*, vol. 213, pp. 153-161, 2016 https://doi.org/10.1016/j.molliq.2015.11.015.

[26] M. Sheikholeslami and A. J. Chamkha, "Electrohydrodynamic free convection heat transfer of a nanofluid in a semi-annulus enclosure with a sinusoidal wall," *Numerical Heat Transfer, Part A: Applications*, vol. 69, no. 7, pp. 781-793, 2016. https://doi.org/10.1080/10407782.2015.1090819.

[27] D. Jing and Y. Pan, "Electroviscous effect and convective heat transfer of pressure-driven flow through microtubes with surface charge-dependent slip," *International Journal of Heat and Mass Transfer*, vol. 101, pp. 648-655, 2016. https://doi.org/10.1016/j.ijheatmasstransfer.2016.05.087.

[28] M. Amiri, M. B. Ayani, P. Ziolkowski, and D. Mikielewicz, "Numerical analysis of vacuum drying of a porous body in the integrated domain," *Journal of Food Process Engineering*, vol. 45, no. 4, p. e14006, 2022. https://doi.org/10.1111/jfpe.14006

[29] S. Zadhossein *et al.*, "Exergy and energy analyses of microwave dryer for cantaloupe slice and prediction of thermodynamic parameters using ANN and ANFIS algorithms," *Energies*, vol. 14, no. 16, p. 4838, 2021. https://doi.org/10.3390/en14164838

[30] M. Amiri and M. B. Ayani, "The effect of heat and mass transfer coefficients on the vacuum drying of porous body, a numerical study," *Journal of Middle East Applied Science and Technology*, vol. 4, 2014. https://profdoc.um.ac.ir/paper-abstract-1040147.html

[31] M. Sheikholeslami and R. Ellahi, "Electrohydrodynamic nanofluid hydrothermal treatment in an enclosure with sinusoidal upper wall," *Applied Sciences*, vol. ,5no. 3, pp. 294-306, 2015. https://doi.org/10.3390/app5030294.

[32] G. Leonard, M. Mitchner, and S. Self, "An experimental study of the electrohydrodynamic flow in electrostatic precipitators," *Journal of Fluid Mechanics*, vol. 127, pp. 123-140, 1983. https://doi.org/10.1017/S0022112083002657.

[33] L. Zhao and K. Adamiak, "EHD flow in air produced by electric corona discharge in pin–plate configuration," *Journal of electrostatics*, vol. 63, no. 3-4, pp. 337-350, 2005. https://doi.org/10.1016/j.elstat.2004.06.003.

[34] P. Béquin, K. Castor, and J. Scholten, "Electric wind characterisation in negative point-to-plane corona discharges in air," *The European Physical Journal-Applied Physics*, vol. 22, no. 1, pp. 41-49, 2003. https://doi.org/10.1051/epjap:2003006.

[35] G. Kallio and D. Stock, "Interaction of electrostatic and fluid dynamic fields in wire—plate electrostatic precipitators," *Journal of Fluid Mechanics*, vol. ,240pp. 133-166, 1992. https://doi.org/10.1017/S0022112092000053.

[36] A. Soldati and S. Banerjee, "Turbulence modification by large-scale organized electrohydrodynamic flows," *Physics of Fluids,* vol. 10, no. 7, pp. 1742-1756, 1998. https://doi.org/10.1063/1.869691.

[37] H. M. Deylami, N. Amanifard, F. Dolati, R. Kouhikamali, and K. Mostajiri, "Numerical investigation of using various electrode arrangements for amplifying the EHD enhanced heat transfer in a smooth channel," *Journal of Electrostatics,* vol. 71, no. 4, pp. 656-665, 2013. https://doi.org/10.1016/j.elstat.2013.03.007.

[38] M. Peng, T.-H. Wang, and X.-D. Wang, "Effect of longitudinal electrode arrangement on EHD-induced heat transfer enhancement in a rectangular channel," *International Journal of Heat and Mass Transfer*, vol. 93, pp. 1072-1081, 2016. https://doi.org/10.1016/j.ijheatmasstransfer.2015.10.043.

[39] T.-H. Wang, M. Peng, X.-D. Wang, and W.-M. Yan, "Investigation of heat transfer enhancement by electrohydrodynamics in a double-wall-heated channel," *International Journal of Heat and Mass Transfer,* vol. 113, pp. 373-383, 2017. https://doi.org/10.1016/j.ijheatmasstransfer.2017.05.079.

[40] H. Moayedi, N. Amanifard, and H. M. Deylami, "Evaluation of using micropolar fluid approach for the EHD-enhanced forced convection through a rectangular channel using multiple electrode arrangements," *Applied Thermal Engineering*, vol. 159, p. 113857, 2019. https://doi.org/10.1016/j.applthermaleng.2019.113857.

[41] P. Sivashanmugam, "Application of nanofluids in heat transfer," *An overview of heat transfer phenomena*, vol. 16, 2012. http://dx.doi.org/10.5772/2623

[42] S. K. Das, S. U. Choi, and H. E. Patel, "Heat transfer in nanofluids—a review," *Heat transfer engineering*, vol. 27, no. 10, pp. 3-19, 2006. https://doi.org/10.1080/01457630600904593.

[43] G. Liang and I. Mudawar, "Review of pool boiling enhancement with additives and nanofluids," *International Journal of Heat and Mass Transfer,* vol. 124, pp. 423-453, 2018. https://doi.org/10.1016/j.ijheatmasstransfer.2018.03.046.

[44] A. Nazari and S. Saedodin, "An experimental study of the nanofluid pool boiling on the aluminium surface," *Journal of Thermal Analysis and Calorimetry*, vol. 135, no. 3, pp. 1753-1762, 2019. https://doi.org/10.1007/s10973-018-7609-9.

[45] H. Park, S. J. Lee, and S. Y. Jung, "X-ray imaging analysis on behaviors of boiling bubbles in nanofluids," *International Journal of Heat and Mass Transfer*, vol. 128, pp. 443-449, 2019. https://doi.org/10.1016/j.ijheatmasstransfer.2018.09.015.

[46] H. Park, S. J. Lee, and S. Y. Jung, "Effect of nanofluid formation methods on behaviors of boiling bubbles," *International Journal of Heat and Mass Transfer*, vol. 135, pp. 1312-1318, 2019. https://doi.org/10.1016/j.ijheatmasstransfer.2019.02.091.

[47] M. Boussoufi and A. Sabeur, "Natural convective nanofluid flow characteristics with Brownian motion effect in an annular space between confocal elliptic cylinders," *Numerical Heat Transfer, Part A: Applications*, pp. 1-16, 2022. https://doi.org/10.1080/10407782.2022.2102396

[48] M. Sheikholeslami and D. Ganji, "Nanofluid convective heat transfer using semi analytical and numerical approaches: a review," *Journal of the Taiwan Institute of Chemical Engineers,* vol. 65, pp. 43-77, 2016. https://doi.org/10.1016/j.jtice.2016.05.014.

[49] M. Bouhalleb and H. Abbassi, "Natural convection in an inclined rectangular enclosure filled by CuO–H2O nanofluid, with sinusoidal temperature distribution," *International Journal of Hydrogen Energy*, vol. 40, no. 39, pp. 13676-13684, 2015. https://doi.org/10.1016/j.ijhydene.2015.04.090.

[50] R. Ahmad and M. Mustafa, "Model and comparative study for rotating flow of nanofluids due to convectively heated exponentially stretching sheet, "*Journal of Molecular Liquids*, vol. 220, pp. 635-641, 2016. https://doi.org/10.1016/j.molliq.2016.04.125.

[51] M. Bouhalleb and H. Abbassi, "Natural convection of nanofluids in enclosures with low aspect ratios," *International journal of hydrogen energy*, vol. 39, no. 27, pp. 15275-15286, 2014. https://doi.org/10.1016/j.ijhydene.2014.04.069.

[52] F. A. Kulacki *et al.*, *Handbook of thermal science and engineering*. Springer, 2018.

[53] L. Cheng, G. Ribatski, and J. R. Thome, "Two-phase flow patterns and flow-pattern maps: fundamentals and applications," *Applied Mechanics Reviews,* vol. 61, no. 5, 2008. https://doi.org/10.1115/1.2955990.

[54] D. Sarker, W. Ding, C. Schneider, and U. Hampel, "Single bubble dynamics during nucleate flow boiling on a vertical heater: Experimental and theoretical analysis of the effect of surface wettability, roughness and bulk liquid velocity," *International Journal of Heat and Mass Transfer,* vol. 142, p. 118481, 2019. https://doi.org/10.1016/j.ijheatmasstransfer.2019.118481.

[55] J. L. Bottini, V. Kumar, S. Hammouti, D. Ruzic, and C. S. Brooks, "Influence of wettability due to laser-texturing on critical heat flux in vertical flow boiling," *International Journal of Heat and Mass Transfer,* vol. 127, pp. 806-817, 2018. https://doi.org/10.1016/j.ijheatmasstransfer.2018.06.113

[56] S. Singh and N. Verma, "Graphitic carbon micronanofibers asymmetrically dispersed with alumina-nickel nanoparticles: a novel electrode for mediatorless microbial fuel cells," *international journal of hydrogen energy,* vol. 40, no. 17, pp. 5928-5938, 2015. https://doi.org/10.1016/j.ijhydene.2015.03.010.

[57] M. Kopp, D. Coleman, C. Stiller, K. Scheffer, J. Aichinger, and B. Scheppat, "Energiepark Mainz: Technical and economic analysis of the worldwide largest Power-to-Gas plant with PEM electrolysis," *International Journal of Hydrogen Energy,* vol. 42, no. 19, pp. 13311-13320, 2017. https://doi.org/10.1016/j.ijhydene.2016.12.145.

[58] A. Fly and R. Thring, "A comparison of evaporative and liquid cooling methods for fuel cell vehicles," *international journal of hydrogen energy,* vol. 41, no. 3 ,2pp. 14217-14229, 2016. https://doi.org/10.1016/j.ijhydene.2016.06.089

[59] M. Nematolahi, B. Behzadinejad, and A. Golestani, "Feasibility study of using nanofluids as a neutron absorber in reactor emergency core cooling system," *International Journal of Hydrogen Energy,* vol. 40, no. 44, pp. 15192-15197. https://doi.org/10.1016/j.ijhydene.2015.03.159..2015 ,

[60] S. Shahnazar, S. Bagheri, and S. B. Abd Hamid, "Enhancing lubricant properties by nanoparticle additives," *International journal of hydrogen energy,* vol. 41, no. 4, pp. 3153-3170, 2016. https://doi.org/10.1016/j.ijhydene.2015.12.040.

[61] A. M. Rashad, M. El-Hakiem, and M. Abdou, "Natural convection boundary layer of a non-Newtonian fluid about a permeable vertical cone embedded in a porous medium saturated with a nanofluid," *Computers & Mathematics with Applications,* vol. 62, no. 8, pp. 3140-3151, 2011. https://doi.org/10.1016/j.camwa.2011.08.027.

[62] B. C. Pak and Y. I. Cho, "Hydrodynamic and heat transfer study of dispersed fluids with submicron metallic oxide particles," *Experimental Heat Transfer an International Journal,* vol. 11, no. 2, pp. 151-170, 1998. https://doi.org/10.1080/08916159808946559.

[63] P. Kumar, R. Dwivedi, and K. Pandey, "Numerical investigation of thermo-hydraulic transport characteristics of laminar flow through partially filled porous wavy channel: Effect of Prandtl number," *Numerical Heat Transfer, Part A: Applications,* pp. 1-22, 2022. https://doi.org/10.1080/10407782.2022.2102342

[64] Y. Xuan and W. Roetzel, "Conceptions for heat transfer correlation of nanofluids," *International Journal of heat and Mass transfer,* vol. 43, no. 19, pp. 3701-3707, 2000. https://doi.org/10.1016/S0017-9310(99)00369-5.

[65] M. Memari, E. Boumari, A. Shoghi, H. Maddah, M. H. Ahmadi, and M. Sharifpur, "Numerical investigation of heat transfer in a tube equipped with twisted tape with different angles and under constant heat flux with copper nanofluid and evaluation of the results obtained using perceptron artificial neural networks," *Numerical Heat Transfer, Part A: Applications,* pp. 1-24, 2022. https://doi.org/10.1080/10407782.2022.2068879

[66] H. C. Brinkman, "The viscosity of concentrated suspensions and solutions," *The Journal of chemical physics,* vol. 20, no. 4, pp. 571-571, 1952. https://doi.org/10.1063/1.1700493.

[67] J. C. Maxwell, *A treatise on electricity and magnetism*. Clarendon press, 1873.

[68] R. Hamilton and O. Crosser, "Ind. Eng. Chem. Fundam," ed, 1962.

[69] A. Moradian and M. S. Saidi, "Electrohydrodynamically enhanced nucleation phenomenon: a theoretical study," *Journal of Enhanced Heat Transfer,* vol. 15, no. 1, 2008. DOI: 10.1615/JEnhHeatTransf.v15.i1.10.

[70] V. Viktorov and M. Nimafar, "A novel generation of 3D SAR-based passive micromixer: efficient mixing and low pressure drop at a low Reynolds number," *Journal of Micromechanics and Microengineering,* vol. 23, no. 5, p. 055023, 2013. Doi:10.1088/0960-1317/23/5/055023.